Computational Geosciences (2020) 24:1031–1055
https://doi.org/10.1007/s10596-019-09909-5

ORIGINAL PAPER

A posteriori error estimates for a compositional two-phase flow with nonlinear complementarity constraints

Ibtihel Ben Gharbia[1] · Jad Dabaghi[2,3] · Vincent Martin[4] · Martin Vohralík[2,3]

Received: 10 November 2018 / Accepted: 10 October 2019 / Published online: 10 January 2020

Abstract

In this work, we develop an a posteriori-steered algorithm for a compositional two-phase flow with exchange of components between the phases in porous media. As a model problem, we choose the two-phase liquid–gas flow with appearance and disappearance of the gas phase formulated as a system of nonlinear evolutive partial differential equations with nonlinear complementarity constraints. The discretization of our model is based on the backward Euler scheme in time and the finite volume scheme in space. The resulting nonlinear system is solved via an inexact semismooth Newton method. The key ingredients for the a posteriori analysis are the discretization, linearization, and algebraic flux reconstructions allowing to devise estimators for each error component. These enable to formulate criteria for stopping the iterative algebraic solver and the iterative linearization solver whenever the corresponding error components do not affect significantly the overall error. Numerical experiments are performed using the Newton-min algorithm as well as the Newton–Fischer–Burmeister algorithm in combination with the GMRES iterative linear solver to show the efficiency of the proposed adaptive method.

Keywords Compositional multiphase flow · Phase transition · Complementarity condition · Semismooth Newton method · A posteriori error estimate · Adaptivity · Stopping criterion

1 Introduction

The storage of radioactive waste in deep geological layers generates broad interest among researchers and engineers concerned with the ecosystem preservation and protection. This storage induces, on a long time-scale, a gas (hydrogen) emission affecting heavily the environment and its sustainable and renewable resources. The mathematical models describing these complex phenomena are part of the large category of strongly nonlinear evolutive multiphase multi-compositional equations where numerical simulation appears to be the only viable approach to finding a solution. A key point investigated today is the reduction of the computational cost of the numerical resolution employing an adaptive strategy based on a posteriori error estimates [26, 29, 30, 32, 72].

In this work, we consider a simpler situation described by a compositional two-phase flow in an isotropic porous medium in two space dimensions. The two miscible fluids involved are liquid and gas, and exchange components. To be coherent with the physical aspects of the problem, at the beginning of the simulation, the medium is monophasic liquid, i.e., completely filled with the water component (the amount of hydrogen is negligible and completely dissolved in the liquid). Afterwards, the quantity of hydrogen increases, and it will be partially gaseous. At this stage, the flow is two-phase liquid–gas. In a usual scenario, at the end of the simulation, the production of gas hydrogen stops and the medium comes back to monophasic liquid.

✉ Jad Dabaghi
jad.dabaghi@inria.fr

Ibtihel Ben Gharbia
ibtihel.ben-gharbia@ifpen.fr

Vincent Martin
vincent.martin@utc.fr

Martin Vohralík
martin.vohralik@inria.fr

[1] IFP Energies Nouvelles, 1 & 4 av. Bois Préau, 92852 Rueil-Malmaison, France

[2] Inria, 2 rue Simone Iff, 75589 Paris, France

[3] Université Paris-Est, CERMICS (ENPC), 77455 Marne-la-Vallée 2, France

[4] Université Technologie de Compiègne (UTC), Compiègne 60200, France

The mathematical model expressing the behavior of two fluids with or without components in a porous medium relies on a strongly nonlinear system of partial differential equations where the unknowns are the pressure and saturation of the phases (see the book of Chen et al. [21]). In Chavent and Jaffré [18], a reduction of these two-phase (without components) equations to a system of a single parabolic saturation equation coupled with an elliptic pressure equation is introduced, replacing the two pressure unknowns (one per phase) by only one pressure unknown, called the global pressure. A formulation for the compositional compressible two-phase flow liquid–gas by the global pressure has been recently proposed in Amaziane et al. [2]. Another formulation providing interesting results is the method of negative saturations (see Panfilov and Rasoulzadeh [57] and Panfilov and Panfilova [56]).

Concerning the numerical methods employed for the discretization of the compositional multiphase models, we mention the finite differences, finite volumes, finite elements, mixed finite elements, and discontinuous Galerkin methods (see the books [6, 18, 20, 21, 41, 68] and the references therein for a general introduction). The finite volume method is a popular approach and is commonly used in practice as it satisfies by construction local mass balance and is easy to implement (see [23, 35, 43]).

One difficulty encountered by engineers is in handling the appearance/disappearance of the phases. From a mathematical standpoint, we can mention the pioneering works of [25] and [39] that are relevant for compositional multiphase flows. Nevertheless, it often leads to irregular convergence behavior if the phase states are quickly changing. More recently, the approach consists in formulating the phase transitions as a set of local inequality constraints, which are then directly integrated into the nonlinear solver using nonlinear complementarity conditions. For a two- phase industrial application, we can mention the work of Bourgeat et al. [14], Lauser et al. [52], and Jaffré and Sboui [67] where in the last reference the appearance and disappearance of the gas phase are treated by Henry's law giving rise to a system of nonlinear equations coupled with nonlinear complementarity conditions. Next, in Ben Gharbia and Jaffré [12], the same approach is introduced with as main novelty the application of an exact semismooth Newton solver to treat the nonlinearities on the complementarity constraints.

Usually, the nonlinear system is not solved exactly, leading to the concept of an inexact semismooth Newton method which is a popular approach to speed-up the convergence. Such approaches can be found in [27, 31, 47] for the case of inexact Newton methods and in [36, 40, 45, 53] for inexact semismooth Newton methods. For convergence results of semismooth Newton algorithms, refer to [9–11, 37, 38]. For two-phase flows, other linearization methods are possible and successfully used in practice. We can mention, as an alternative to Newton's method, the recent work of Radu et al. [62] based on [60, 69]. Therein, a linear convergent L-scheme linearization procedure for Lipschitz-continuous saturations that does not involve the calculations of any derivatives and does not need a regularization step is developed. Numerical convergence of the L-scheme is also observed with monotone increasing Hölder continuous saturations.

In this work, we use the mathematical model of [12] and we are interested in deriving a posteriori error estimates, in order to formulate adaptive stopping criteria for our inexact semismooth solvers to save computational time. There is a well-developed literature on a posteriori error estimates for partial differential equations. Related to our formulation, we first mention the fundamental work of Prager and Synge [61], the books of Ainsworth and Oden [1] and Repin [64], and the work of Ladevèze [51], where upper bounds for the error inspired from Prager and Synge's identity are derived. More recently, one approach consists in obtaining the so-called potential and equilibrated flux reconstructions solving auxiliary local problems (see Destuynder and Métivet [28], Braess and Schöberl [15], Ern and Vohralík [33], and the references therein).

Concerning a posteriori error estimate for variational inequalities, one can point out the pioneering work of Kornhuber [48], Chen and Nochetto [22], Veeser [70], Repin [65], and Ben Belgacem et al. [8]. In particular in [8], a posteriori error estimates are given for exact solvers and recently, in [26], a posteriori error estimates are derived for inexact semismooth solvers and provide adaptive stopping criteria. The concept of adaptive stopping criteria relies on stopping the nonlinear and linear iterations whenever the associated estimators do not affect significantly the overall error (see [5, 26, 32, 44, 54]). For multiphase flows, devising a posteriori error estimates between the exact solution and approximate solution seems very ambitious and is still an open problem. Indeed, the existence of a weak solution relies on several strong assumptions and to construct upper bounds for energy norm errors seems somewhat inaccessible. In [17], an estimation between the exact solution and the approximate solution for the L^2 norm in time and H^{-1} in space has been derived in the case of a two-phase flow with only one component per phase. In general, for multiphase compositional flows, the alternative is to construct estimators as upper bounds for some dual norm of a residual (see [29], [30], and [72]). Constructing a posteriori error estimates and devising adaptive stopping criteria for inexact semismooth Newton solvers when the phase transition occurs has never been presented to the best of our knowledge. Therefore, we will try to fill this gap.

We organize our paper as follows. In Sections 2 and 3, we introduce the model problem, its finite difference

discretization in time, and its finite volume discretization in space. Next, in Section 4, we show that any inexact semismooth Newton method can be employed to solve the nonlinear system stemming from the discretization. Section 5 is devoted to the description of the various potential and flux reconstruction enabling to obtain a posteriori error estimators distinguishing all error components, namely the discretization error, the semismooth linearization error, and the algebraic error. In Section 6, we show numerical experiments when the semismooth min and Fischer–Burmeister solvers are employed in one-dimensional space, and Section 7 summarizes our findings.

2 Setting

The methodology is presented for the sake of clarity in 2 space dimensions but can be extended to 3 or 1 without difficulties. We assume that the porous medium domain Ω is an open bounded connected polygon. We are interested in solving the model of appearance/disappearance of the gas phase thanks to nonlinear complementarity conditions over the time interval $(0, t_F)$, $t_F > 0$, and devise a posteriori error estimates.

2.1 Functional spaces

First, we recall the definition of some Sobolev spaces. Let $H^1(\Omega)$ be the space of L^2 functions on the domain Ω which admit a weak gradient in $[L^2(\Omega)]^2$ and $H_0^1(\Omega)$ its zero-trace subspace. Similarly, $\mathbf{H}(\mathrm{div}, \Omega)$ stands for the space of $[L^2(\Omega)]^2$ functions having a weak divergence in $L^2(\Omega)$. The standard notation ∇ and $\nabla\cdot$ are used respectively for the weak gradient and divergence. For a nonempty bounded set $\mathcal{O}$ of $\mathbb{R}^2$, we denote its Lebesgue measure by $|\mathcal{O}|$ and the $L^2(\mathcal{O})$ scalar product by $(u, v)_{\mathcal{O}} = \int_{\mathcal{O}} uv \, \mathrm{dx}$ for $u, v \in L^2(\mathcal{O})$. We also use the following notations: $\|v\|_{\mathcal{O}}^2 := (v, v)_{\mathcal{O}}$, and $\|\nabla v\|_{\mathcal{O}}^2 := (\nabla v, \nabla v)_{\mathcal{O}}$. Besides, the Poincaré–Friedrichs and the Poincaré–Wirtinger inequalities (see [7, 59]), state that if $\overline{v}_{\mathcal{O}}$ denotes the mean value of v on $\mathcal{O}$ and $h_{\mathcal{O}}$ the diameter of $\mathcal{O}$, then

$$\|v\|_{\mathcal{O}} \le C_{\mathrm{PF}} h_{\mathcal{O}} \|\nabla v\|_{\mathcal{O}} \quad \forall v \in H_0^1(\mathcal{O}),$$
$$\|v - \overline{v}_{\mathcal{O}}\|_{\mathcal{O}} \le C_{\mathrm{PW}} h_{\mathcal{O}} \|\nabla v\|_{\mathcal{O}} \, \forall v \in H^1(\mathcal{O}).$$

The constants C_{PF} and C_{PW} can be precisely estimated in many cases. In particular, if $\mathcal{O}$ is convex, C_{PW} can be taken as $\frac{1}{\pi}$, see [7, 59] whereas $C_{\mathrm{PF}} = 1$ is always possible.

2.2 The compositional two-phase model

We consider a compositional thermal biphasic flow in the porous medium Ω. The porous medium is characterized by its porosity ϕ and its absolute permeability $\underline{\mathbf{K}}$, both of which are assumed constant in space and time for the sake of simplicity. When the porous medium Ω is anisotropic, the positive constant $\underline{\mathbf{K}}$ is replaced by a symmetric positive definite matrix.

The phases are collected in the set $\mathscr{P} = \{\mathrm{l}, \mathrm{g}\}$ where "l" stands for the liquid phase and "g" for the gas one. Each of the considered fluids can be composed of two components: water (denoted by "w") and hydrogen (denoted by "h"). The set of components is defined by $\mathscr{C} = \{\mathrm{w}, \mathrm{h}\}$ and we denote by $\mathscr{C}^p$ the set of components present in the phase p and $\mathscr{P}_c$ the set of phases containing the component c.

For a given phase $p \in \mathscr{P}$, S^p denotes its saturation, P^p its pressure and for each component $c \in \mathscr{C}^p$, χ_c^p is the molar fraction of the component c in phase p. Because of the interactions of forces between the fluids and the solid matrix and the curvature of the surface contact between the two fluids, we have an additional pressure called the capillary pressure depending on the saturation S^{l} with higher wettability (see [55]), defined as

$$P_{\mathrm{cp}}(S^{\mathrm{l}}) = P^{\mathrm{g}} - P^{\mathrm{l}}. \tag{1}$$

Here, P_{cp} is a given function of the liquid saturation S^{l} and in the literature, the suggestions of Brooks and Corey or Van Genuchten are commonly used, see [42]. The unknowns of the model below will be S^{l} (saturation of the liquid phase), P^{l} (pressure of the liquid phase), and $\chi_{\mathrm{h}}^{\mathrm{l}}$ (molar fraction of hydrogen in the liquid phase).

For a phase $p \in \mathscr{P}$ and for a given component $c \in \mathscr{C}^p$, $\rho_c^p(P^p, \chi_c^p)$ represents its molar density, $C_c^p(P^p, \chi_c^p)$ its molar concentration, $\mathbf{J}_c^p(P^p, S^p, \chi_c^p)$ its Fick flux, and D_c^p its molecular diffusion coefficient supposed constant. Furthermore, for a given phase $p \in \mathscr{P}$, $\mu^p(P^p, \chi_c^p)$ stands for its dynamic viscosity and $k_{\mathrm{r}}^p(S^p)$ represents its relative permeability. The relative permeability is typically an increasing function of S^p satisfying $k_{\mathrm{r}}^p(0) = 0$. We do not specify here the assumptions on this and the other nonlinear functions; instead we suppose below in Assumption 2 that all the data of the model are such that they allow for an appropriate definition of the weak solution (see also Remark 1). Examples of possible model parameters are then given in Section 6. Then, M_c represents the molar mass of the component c and $g = 9.81\mathrm{m.s}^{-2}$ is the gravity acceleration constant. We recall some elementary properties. The molar density of phase $p \in \mathscr{P}$ is defined as the sum of the molar densities of the components present in the phase:

$$\rho^p := \rho_{\mathrm{w}}^p + \rho_{\mathrm{h}}^p.$$

The molar concentration of phase $p \in \mathscr{P}$ is defined as the sum of the molar concentrations of the components present in the phase:

$$C^p := C^p_{\mathrm{w}} + C^p_{\mathrm{h}} := \frac{\rho^p_{\mathrm{w}}}{M_{\mathrm{w}}} + \frac{\rho^p_{\mathrm{h}}}{M_{\mathrm{h}}}. \tag{2}$$

Furthermore, the molar fraction of component $c \in \mathscr{C}^p$ is defined by

$$\chi^p_c := \frac{C^p_c}{C^p}, \quad \text{so that} \quad \chi^p_{\mathrm{w}} + \chi^p_{\mathrm{h}} = 1. \tag{3}$$

The Fick's law for any component $c \in \mathscr{C}^p$ gives

$$\mathbf{J}^p_c := -\phi M_c S^p C^p D^p_c \nabla \chi^p_c.$$

The molecular diffusion in a phase $p \in \mathscr{P}$ is supposed negligible compared to the global displacement of this phase which implies

$$\mathbf{J}^p_{\mathrm{h}} + \mathbf{J}^p_{\mathrm{w}} = 0. \tag{4}$$

Next, as the pores are completely occupied by the fluids, we have the closure equation

$$S^{\mathrm{l}} + S^{\mathrm{g}} = 1. \tag{5}$$

To finish, the Darcy velocity $\mathbf{q}^p$ for any phase $p \in \mathscr{P}$ is defined by:

$$\mathbf{q}^p := -\underline{\mathbf{K}} \frac{k^p_{\mathrm{r}}(S^p)}{\mu^p} \left[\nabla P^p - \rho^p g \nabla z\right].$$

We make the following assumptions:

Assumption 1 *We assume that the fluid is at thermodynamic equilibrium and that the water is incompressible and only present in the liquid phase:*

$\rho^{\mathrm{l}}_{\mathrm{w}}$ *is a constant,* $\rho^{\mathrm{g}}_{\mathrm{w}} = 0$, $\rho^{\mathrm{g}} = \rho^{\mathrm{g}}_{\mathrm{h}}$, $\chi^{\mathrm{g}}_{\mathrm{h}} = 1$, *and* $\chi^{\mathrm{g}}_{\mathrm{w}} = 0$.

Next, we suppose that the liquid solution is an ideal diluted solution and the gas is slightly compressible:

$C^{\mathrm{l}}_{\mathrm{h}} \ll C^{\mathrm{l}}_{\mathrm{w}}$ *and* $\rho^{\mathrm{g}} = \beta^{\mathrm{g}} P^{\mathrm{g}}$,

where β^{g} *is a compressibility constant.*

From Assumption 1 and (4), we obtain $\mathbf{J}^{\mathrm{g}}_{\mathrm{h}} = \mathbf{J}^{\mathrm{g}}_{\mathrm{w}} = 0$. Next, equation (3) combined with Assumption 1 gives

$$\chi^{\mathrm{l}}_{\mathrm{w}} \approx 1 \quad \text{and} \quad \chi^{\mathrm{l}}_{\mathrm{h}} \approx \frac{C^{\mathrm{l}}_{\mathrm{h}}}{C^{\mathrm{l}}_{\mathrm{w}}}. \tag{6}$$

Finally, equations (2) and (6) yield

$$\rho^{\mathrm{l}}_{\mathrm{h}} \approx \beta^{\mathrm{l}} \chi^{\mathrm{l}}_{\mathrm{h}} \quad \text{with} \quad \beta^{\mathrm{l}} = \rho^{\mathrm{l}}_{\mathrm{w}} \frac{M_{\mathrm{h}}}{M_{\mathrm{w}}}. \tag{7}$$

Under Assumption 1, Fick's law for the hydrogen component in the liquid phase reads

$$\mathbf{J}^{\mathrm{l}}_{\mathrm{h}} = -\phi M_{\mathrm{h}} S^{\mathrm{l}} \left(\frac{\rho^{\mathrm{l}}_{\mathrm{w}}}{M_{\mathrm{w}}} + \frac{\beta^{\mathrm{l}}}{M_{\mathrm{h}}} \chi^{\mathrm{l}}_{\mathrm{h}} \right) D^{\mathrm{l}}_{\mathrm{h}} \nabla \chi^{\mathrm{l}}_{\mathrm{h}}, \tag{8}$$

and the Darcy velocities read

$$\begin{aligned} \mathbf{q}^{\mathrm{l}} &= -\underline{\mathbf{K}} \frac{k^{\mathrm{l}}_{\mathrm{r}}(S^{\mathrm{l}})}{\mu^{\mathrm{l}}} \left[\nabla P^{\mathrm{l}} - \left[\rho^{\mathrm{l}}_{\mathrm{w}} + \beta^{\mathrm{l}} \chi^{\mathrm{l}}_{\mathrm{h}}\right] g \nabla z\right], \\ \mathbf{q}^{\mathrm{g}} &= -\underline{\mathbf{K}} \frac{k^{\mathrm{g}}_{\mathrm{r}}(1 - S^{\mathrm{l}})}{\mu^{\mathrm{g}}} \left[\nabla \left[P^{\mathrm{l}} + P_{\mathrm{cp}}(S^{\mathrm{l}})\right] \right. \\ &\quad \left. - \beta^{\mathrm{g}} \left[P^{\mathrm{l}} + P_{\mathrm{cp}}(S^{\mathrm{l}})\right] g \nabla z\right]. \end{aligned} \tag{9}$$

In the sequel, all approximate equations will be considered to be exact equations.

2.3 Governing partial differential equations and nonlinear complementarity constraints

The system of partial differential equation representing the mass conservation for the two components, water and hydrogen, has the following form:

$$\begin{aligned} \partial_t(\phi \rho^{\mathrm{l}}_{\mathrm{w}} S^{\mathrm{l}} + \phi \rho^{\mathrm{g}}_{\mathrm{w}} S^{\mathrm{g}}) + \nabla \cdot (\rho^{\mathrm{l}}_{\mathrm{w}} \mathbf{q}^{\mathrm{l}} + \rho^{\mathrm{g}}_{\mathrm{w}} \mathbf{q}^{\mathrm{g}} + \mathbf{J}^{\mathrm{l}}_{\mathrm{w}} + \mathbf{J}^{\mathrm{g}}_{\mathrm{w}}) &= Q_{\mathrm{w}}, \\ \partial_t(\phi \rho^{\mathrm{l}}_{\mathrm{h}} S^{\mathrm{l}} + \phi \rho^{\mathrm{g}}_{\mathrm{h}} S^{\mathrm{g}}) + \nabla \cdot (\rho^{\mathrm{l}}_{\mathrm{h}} \mathbf{q}^{\mathrm{l}} + \rho^{\mathrm{g}}_{\mathrm{h}} \mathbf{q}^{\mathrm{g}} + \mathbf{J}^{\mathrm{l}}_{\mathrm{h}} + \mathbf{J}^{\mathrm{g}}_{\mathrm{h}}) &= Q_{\mathrm{h}}, \end{aligned} \tag{10}$$

where Q_c is a source term representing the outflow of the component $c \in \mathscr{C}$. To model the appearance of the gas phase, we employ Henry's law (see [12, 67]), giving

$$H P^{\mathrm{g}} = \rho^{\mathrm{l}}_{\mathrm{h}},$$

with $H = \tilde{H} M_{\mathrm{h}}$ where $\tilde{H}$ is Henry's constant. Next, using (5), (1), and (7) yields

$$1 - S^{\mathrm{l}} > 0 \quad \text{and} \quad H[P^{\mathrm{l}} + P_{\mathrm{cp}}(S^{\mathrm{l}})] - \beta^{\mathrm{l}} \chi^{\mathrm{l}}_{\mathrm{h}} = 0. \tag{11}$$

If the gas phase does not exist, using (5), (1), and [67, Section 3.2], we get

$$1 - S^{\mathrm{l}} = 0 \quad \text{and} \quad H P^{\mathrm{l}} - \beta^{\mathrm{l}} \chi^{\mathrm{l}}_{\mathrm{h}} > 0. \tag{12}$$

Thus, using (11) and (12), we get nonlinear complementarity constraints:

$$\begin{aligned} &1 - S^{\mathrm{l}} \geq 0, \quad H[P^{\mathrm{l}} + P_{\mathrm{cp}}(S^{\mathrm{l}})] - \beta^{\mathrm{l}} \chi^{\mathrm{l}}_{\mathrm{h}} \geq 0, \\ &[1 - S^{\mathrm{l}}] \left[H[P^{\mathrm{l}} + P_{\mathrm{cp}}(S^{\mathrm{l}})] - \beta^{\mathrm{l}} \chi^{\mathrm{l}}_{\mathrm{h}}\right] = 0. \end{aligned} \tag{13}$$

Finally, using Assumption 1, (10), and (13), our two-phase flow model with exchange between phases is governed by the following system: find S^{l}, P^{l}, $\chi^{\mathrm{l}}_{\mathrm{h}}$ such that

$$\begin{aligned} &\partial_t l_{\mathrm{w}} + \nabla \cdot \boldsymbol{\Phi}_{\mathrm{w}} = Q_{\mathrm{w}}, \\ &\partial_t l_{\mathrm{h}} + \nabla \cdot \boldsymbol{\Phi}_{\mathrm{h}} = Q_{\mathrm{h}}, \\ &1 - S^{\mathrm{l}} \geq 0, \ H[P^{\mathrm{l}} + P_{\mathrm{cp}}(S^{\mathrm{l}})] - \beta^{\mathrm{l}} \chi^{\mathrm{l}}_{\mathrm{h}} \geq 0, \\ &[1 - S^{\mathrm{l}}] \left[H[P^{\mathrm{l}} + P_{\mathrm{cp}}(S^{\mathrm{l}})] - \beta^{\mathrm{l}} \chi^{\mathrm{l}}_{\mathrm{h}}\right] = 0. \end{aligned} \tag{14}$$

Here, the component fluxes $\boldsymbol{\Phi}_c$, $c \in \mathscr{C}$, are defined by

$$\boldsymbol{\Phi}_{\mathrm{w}} = \rho^{\mathrm{l}}_{\mathrm{w}} \mathbf{q}^{\mathrm{l}} - \mathbf{J}^{\mathrm{l}}_{\mathrm{h}}, \tag{15}$$

$$\boldsymbol{\Phi}_{\mathrm{h}} = \beta^{\mathrm{l}} \chi^{\mathrm{l}}_{\mathrm{h}} \mathbf{q}^{\mathrm{l}} + \beta^{\mathrm{g}} \left[P^{\mathrm{l}} + P_{\mathrm{cp}}(S^{\mathrm{l}})\right] \mathbf{q}^{\mathrm{g}} + \mathbf{J}^{\mathrm{l}}_{\mathrm{h}}, \tag{16}$$

where $\mathbf{q}^{\mathrm{l}}$, $\mathbf{q}^{\mathrm{g}}$, and $\mathbf{J}_{\mathrm{h}}^{\mathrm{l}}$ are defined in (9) and (8) and the amounts of components w and h per unit volume are defined by

$$\begin{aligned} l_{\mathrm{w}} &= \phi\rho_{\mathrm{w}}^{\mathrm{l}} S^{\mathrm{l}}, \\ l_{\mathrm{h}} &= \phi\beta^{\mathrm{l}}\chi_{\mathrm{h}}^{\mathrm{l}} S^{\mathrm{l}} + \phi\beta^{\mathrm{g}}\left[P^{\mathrm{l}} + P_{\mathrm{cp}}(S^{\mathrm{l}})\right]\left[1 - S^{\mathrm{l}}\right]. \end{aligned} \tag{17}$$

For the sake of simplicity, we assume that no-flow boundary conditions are prescribed for all the component fluxes,

$$\boldsymbol{\Phi}_c \cdot \boldsymbol{n}_\Omega = 0 \quad \text{on} \quad \partial\Omega \times (0, t_{\mathrm{F}}) \quad c \in \{\mathrm{w}, \mathrm{h}\}$$

with $\boldsymbol{n}_\Omega$ the outward unit normal vector to Ω. At $t = 0$, we prescribe the initial amount of each component

$$l_c(\cdot, 0) = l_c^0 \quad \forall c \in \{\mathrm{w}, \mathrm{h}\}. \tag{18}$$

3 Discretization and numerical approximation

We present in this section the discretization of our model. We use the backward Euler scheme in time and the cell-centered lowest order finite volume scheme in space.

3.1 Space-time meshes

For the time discretization, we consider an increasing sequence of points $\{t_n\}_{0\le n\le N_t}$ such that $t_0 = 0$, $t_{N_t} = t_{\mathrm{F}}$, and we introduce the interval $I_n = (t_{n-1}, t_n)$ and the time step $\tau_n = t_n - t_{n-1}$, $\forall 1 \le n \le N_t$. For the space discretization, we consider $\mathscr{T}_h$ a family of conforming triangular meshes of the space domain Ω. We assume that $\mathscr{T}_h$ is formed by a set of triangles verifying $\bigcup_{K\in\mathscr{T}_h} \overline{K} = \overline{\Omega}$ where the intersection of two elements of $\mathscr{T}_h$ is either an empty set, a vertex, or an edge. We also define $H^1(\mathscr{T}_h)$ as the broken Sobolev space of L^2 functions on the domain Ω such that their restriction to any element K are H^1 in the element K. We denote by $\mathbb{P}_m^{\mathrm{c}}(\mathscr{T}_h)$ the space of continuous piecewise polynomials of degree $\le m$ and by $\mathbb{P}_m^{\mathrm{d}}(\mathscr{T}_h)$ the broken polynomial space of discontinuous piecewise polynomials of degree $\le m$. In the sequel, we will employ $m = 0$ and $m = 2$. We denote by D_m the set of Lagrange degrees of freedom associated to $\mathbb{P}_m^{\mathrm{c}}(\mathscr{T}_h)$.

The set of vertices of $\mathscr{T}_h$ is denoted by $\mathscr{V}_h$ and is decomposed into interior vertices $\mathscr{V}_h^{\mathrm{int}}$ and boundary vertices $\mathscr{V}_h^{\mathrm{ext}}$. The vertices of an element $K \in \mathscr{T}_h$ are collected in the set $\mathscr{V}_K$. We denote by $\mathscr{E}_h$ the set of mesh edges. Boundary edges are collected in the set $\mathscr{E}_h^{\mathrm{ext}} = \{\sigma \in \mathscr{E}_h; \sigma \subset \partial\Omega\}$ and internal edges are collected in the set $\mathscr{E}_h^{\mathrm{int}} = \mathscr{E}_h \backslash \mathscr{E}_h^{\mathrm{ext}}$. Likewise, the edges of an element $K \in \mathscr{T}_h$ are collected in the set $\mathscr{E}_K$ and the later is decomposed into interior edges $\mathscr{E}_K^{\mathrm{int}}$ and boundary edges $\mathscr{E}_K^{\mathrm{ext}}$.

We denote by N_{sp} the number of elements in the mesh $\mathscr{T}_h$. Furthermore, the notation $\boldsymbol{n}_{K,\sigma}$ stands for the outward unit normal vector to the element K on σ. We also assume that the family $\mathscr{T}_h$ is superadmissible in the sense that for all cells $K \in \mathscr{T}_h$ there exists a point $\boldsymbol{x}_K \in K$ (the cell center) and for all edges $\sigma \in \mathscr{E}_h$ there exists a point $\boldsymbol{x}_\sigma \in \sigma$ (the edge center) such that, for all edges $\sigma \in \mathscr{E}_K$, the line segment joining $\boldsymbol{x}_K$ with $\boldsymbol{x}_\sigma$ is orthogonal to σ (see [34]). For an interior edge $\sigma \in \mathscr{E}_h^{\mathrm{int}}$ shared by two elements K and L (denoted in the sequel by $\overline{\sigma} = \overline{K} \cap \overline{L}$), we define the distance between these elements $d_{KL} := \mathrm{dist}(\boldsymbol{x}_K, \boldsymbol{x}_L)$.

Next, the vertical coordinate of any point $\boldsymbol{x}_K$ in the mesh $\mathscr{T}_h$ is denoted by z_K. For $\boldsymbol{a} \in D_m$, we call $\mathscr{T}_{\boldsymbol{a}}$ the patch around $\boldsymbol{a}$, i.e., the set of elements of $\mathscr{T}_h$ that share $\boldsymbol{a}$, and $\omega_h^{\boldsymbol{a}} \subset \Omega$ is the corresponding polygonal subdomain with $\mathbf{n}_{\omega_h^{\boldsymbol{a}}}$ its outward unit normal. The number of elements in $\mathscr{T}_{\boldsymbol{a}}$ is denoted by $|\mathscr{T}_{\boldsymbol{a}}|$. Note for instance that, in 2D, the patch for an interior edge degree of freedom contains exactly 2 elements and the patch for a vertex degree of freedom can contain a variable number of elements.

3.2 Finite volume discretization

Using the cell-centered finite volume method, the unknowns of the model are discretized using one value per cell: $\forall 1 \le n \le N_t$ we let

$$\boldsymbol{U}^n := (\boldsymbol{U}_K^n)_{K\in\mathscr{T}_h} \in \mathbb{R}^{3N_{\mathrm{sp}}}, \qquad \boldsymbol{U}_K^n := \begin{pmatrix} S_K^n \\ P_K^n \\ \chi_K^n \end{pmatrix} \in \mathbb{R}^3,$$

where S_K^n, P_K^n, and χ_K^n are respectively the discrete elementwise unknowns approximating the values of S^{l}, P^{l}, and $\chi_{\mathrm{h}}^{\mathrm{l}}$ in the element $K \in \mathscr{T}_h$. In the same way, $l_{c,K}^n$ approximates the value of l_c in the element $K \in \mathscr{T}_h$.

For a function of time v with sufficient regularity, we denote $v^n := v(t^n)$, $0 \le n \le N_t$, and, for $1 \le n \le N_t$, we define the backward differencing operator

$$\partial_t^n v := \frac{1}{\tau_n}\left(v^n - v^{n-1}\right). \tag{19}$$

To approximate the space gradient we use

$$\left(\boldsymbol{\nabla} v \cdot \boldsymbol{n}_{K,\sigma}, 1\right)_\sigma \approx |\sigma| \frac{v_L - v_K}{d_{KL}} \quad \text{if} \quad \sigma \in \mathscr{E}_K^{\mathrm{int}}, \quad \overline{\sigma} = \overline{K} \cap \overline{L}.$$

First, we discretize the water conservation equation. Let $K \in \mathscr{T}_h$. By integration over the element K, we obtain

$$(\partial_t l_{\mathrm{w}} + \boldsymbol{\nabla} \cdot \boldsymbol{\Phi}_{\mathrm{w}}, 1)_K = (Q_{\mathrm{w}}, 1)_K.$$

The Green formula gives the approximation for $n = 1, \ldots, N_t$

$$|K| \partial_t^n l_{\mathrm{w},K} + \sum_{\sigma\in\mathscr{E}_K} F_{\mathrm{w},K,\sigma}(\boldsymbol{U}^n) = |K| Q_{\mathrm{w,K}}^n, \tag{20}$$

where the discrete elementwise water source term and the discrete elementwise amount of water are given by

$$Q^n_{\mathrm{w,K}} := \int_{I_n} \frac{(Q_\mathrm{w},1)_K}{|K|\tau_n}(t)\,\mathrm{d}t, \quad \text{and} \quad l^n_{\mathrm{w},K} := \phi\rho^{\mathrm{l}}_\mathrm{w} S^n_K \quad \text{and,}$$
$$\partial^n_t l_{\mathrm{w},K} = \frac{1}{\tau_n}\left(l^n_{\mathrm{w},K} - l^{n-1}_{\mathrm{w},K}\right).$$

Let $\sigma \in \mathscr{E}^{\mathrm{int}}_K$, $\overline{\sigma} = \overline{K} \cap \overline{L}$. Then, the total flux across σ of the water component is given by

$$F_{\mathrm{w},K,\sigma}(\boldsymbol{U}^n) := \rho^{\mathrm{l}}_\mathrm{w}(\mathfrak{M}^{\mathrm{l}})^n_\sigma(\psi^{\mathrm{l}})^n_\sigma - (\mathrm{j}^{\mathrm{l}}_\mathrm{h})^n_\sigma, \tag{21}$$

with the discrete Fick term given by

$$(\mathrm{j}^{\mathrm{l}}_\mathrm{h})^n_\sigma := -|\sigma|\phi M_\mathrm{h} S^n_\sigma \left[\frac{\rho^{\mathrm{l}}_\mathrm{w}}{M_\mathrm{w}} + \frac{\beta^{\mathrm{l}}}{M_\mathrm{h}}\chi^n_\sigma\right] D^{\mathrm{l}}_\mathrm{h}\frac{\chi^n_L - \chi^n_K}{d_{KL}}, \tag{22}$$

the discrete liquid Darcy term given by

$$(\psi^{\mathrm{l}})^n_\sigma := -|\sigma|\frac{\mathbf{K}}{d_{KL}}\left[P^n_L - P^n_K - \left[\rho^{\mathrm{l}}_\mathrm{w} + \beta^{\mathrm{l}}\chi^n_\sigma\right] g[z_L - z_K]\right], \tag{23}$$

and the mobility of the liquid phase using an upwind approximation

$$\begin{aligned}(\mathfrak{M}^{\mathrm{l}})^n_\sigma &:= \frac{k^{\mathrm{l}}_\mathrm{r}(S^n_K)}{\mu^{\mathrm{l}}} \quad \text{if} \quad (\psi^{\mathrm{l}})^n_\sigma \geq 0,\\ (\mathfrak{M}^{\mathrm{l}})^n_\sigma &:= \frac{k^{\mathrm{l}}_\mathrm{r}(S^n_L)}{\mu^{\mathrm{l}}} \quad \text{if} \quad (\psi^{\mathrm{l}})^n_\sigma < 0,\end{aligned} \tag{24}$$

where

$$S^n_\sigma := \frac{S^n_K + S^n_L}{2}, \quad \text{and} \quad \chi^n_\sigma := \frac{\chi^n_K + \chi^n_L}{2}. \tag{25}$$

Now, we discretize the hydrogen conservation equation. Let $K \in \mathscr{T}_h$. By integration over the element K we obtain

$$(\partial_t l_\mathrm{h} + \nabla\cdot\boldsymbol{\Phi}_\mathrm{h}, 1)_K = (Q_\mathrm{h}, 1)_K.$$

The Green formula gives the approximation for $n = 1,\ldots,N_t$

$$|K|\partial^n_t l_{\mathrm{h},K} + \sum_{\sigma\in\mathscr{E}_K} F_{\mathrm{h},K,\sigma}(\boldsymbol{U}^n) = |K|Q^n_{\mathrm{h,K}}, \tag{26}$$

where the discrete elementwise hydrogen source term and the discrete elementwise amount of hydrogen are given by

$$\begin{aligned}Q^n_{\mathrm{h,K}} &:= \int_{I_n}\frac{(Q_\mathrm{h},1)_K}{|K|\tau_n}(t)\,\mathrm{d}t,\\ l^n_{\mathrm{h},K} &:= \phi\beta^{\mathrm{l}}\chi^n_K S^n_K + \phi\beta^{\mathrm{g}}\left[P^n_K + P_{\mathrm{cp}}(S^n_K)\right]\left[1 - S^n_K\right].\end{aligned}$$

Let $\sigma \in \mathscr{E}^{\mathrm{int}}_K$, $\sigma = \overline{K}\cap\overline{L}$. The total discrete flux across σ of the hydrogen component is given by

$$\begin{aligned}F_{\mathrm{h},K,\sigma}(\boldsymbol{U}^n) := {}& \beta^{\mathrm{l}}\chi^n_\sigma(\mathfrak{M}^{\mathrm{l}})^n_\sigma(\psi^{\mathrm{l}})^n_\sigma\\ &+ (\mathfrak{M}^{\mathrm{g}})^n_\sigma(\psi^{\mathrm{g}})^n_\sigma(\rho^{\mathrm{g}})^n_\sigma + (\mathrm{j}^{\mathrm{l}}_\mathrm{h})^n_\sigma,\end{aligned} \tag{27}$$

where the discrete Fick term is given by (22), the discrete Darcy liquid term is given by (23), the mobility of the liquid phase is given by (24), and χ^n_σ is given by (25). Furthermore, the discrete Darcy gas term is given by

$$\begin{aligned}(\psi^{\mathrm{g}})^n_\sigma := {}& -|\sigma|\frac{\mathbf{K}}{d_{KL}}\left[P^n_L + P_{\mathrm{cp}}(S^n_L) - P^n_K - P_{\mathrm{cp}}(S^n_K)\right.\\ &\left.-(\rho^{\mathrm{g}})^n_\sigma g[z_L - z_K]\right],\end{aligned}$$

with

$$(\rho^{\mathrm{g}})^n_\sigma := \frac{(\rho^{\mathrm{g}})^n_K + (\rho^{\mathrm{g}})^n_L}{2}, \quad \text{and} \quad (\rho^{\mathrm{g}})^n_K := \beta^{\mathrm{g}}\left[P^n_K + P_{\mathrm{cp}}(S^n_K)\right].$$

Next, the mobility of the gas phase is

$$\begin{aligned}(\mathfrak{M}^{\mathrm{g}})^n_\sigma &:= \frac{k^{\mathrm{g}}_\mathrm{r}(1 - S^n_K)}{\mu^{\mathrm{g}}} \quad \text{if} \quad (\psi^{\mathrm{g}})^n_\sigma \geq 0,\\ (\mathfrak{M}^{\mathrm{g}})^n_\sigma &:= \frac{k^{\mathrm{g}}_\mathrm{r}(1 - S^n_L)}{\mu^{\mathrm{g}}} \quad \text{if} \quad (\psi^{\mathrm{g}})^n_\sigma < 0.\end{aligned}$$

If $\sigma \in \mathscr{E}^{\mathrm{ext}}_K \subset \partial\Omega$, the homogeneous Neumann boundary condition yields

$$F_{\mathrm{w},K,\sigma}(\boldsymbol{U}^n) = F_{\mathrm{h},K,\sigma}(\boldsymbol{U}^n) = 0.$$

Thus, (20) and (26) define $\forall K \in \mathscr{T}_h$, $\forall c \in \{\mathrm{w},\mathrm{h}\}$, $\forall 1 \leq n \leq N_t$ the nonlinear function $H^n_{c,K} : \mathbb{R}^{3N_{\mathrm{sp}}} \to \mathbb{R}$ defined by

$$H^n_{c,K}(\boldsymbol{U}^n) := |K|\partial^n_t l_{c,K} + \sum_{\sigma\in\mathscr{E}^{\mathrm{int}}_K} F_{c,K,\sigma}(\boldsymbol{U}^n) - |K|Q^n_{c,K}. \tag{28}$$

At each time step n, (28) will lead to a system of $2N_{\mathrm{sp}}$ nonlinear equations. As we have $3N_{\mathrm{sp}}$ unknowns, to close the system, we use the nonlinear complementarity conditions as follows.

Let F_K be the function discretizing elementwise $1 - S^{\mathrm{l}}$ and let G_K be the function discretizing elementwise $H[P^{\mathrm{l}} + P_{\mathrm{cp}}(S^{\mathrm{l}})] - \beta^{\mathrm{l}}\chi^{\mathrm{l}}_\mathrm{h}$ defined by:

$$\begin{aligned}F_K : \mathbb{R}^3 &\to \mathbb{R}\\ \boldsymbol{U}^n_K &\longmapsto 1 - S^n_K,\end{aligned}$$

$$\begin{aligned}G_K : \mathbb{R}^3 &\to \mathbb{R}\\ \boldsymbol{U}^n_K &\longmapsto H\left[P^n_K + P_{\mathrm{cp}}(S^n_K)\right] - \beta^{\mathrm{l}}\chi^n_K.\end{aligned}$$

Then, the finite volume scheme corresponding to (14) reads: for all $1 \leq n \leq N_t$, find $\boldsymbol{U}^n \in \mathbb{R}^{3N_{\mathrm{sp}}}$ such that for all $K \in \mathscr{T}_h$

$$\begin{aligned}&H^n_{c,K}(\boldsymbol{U}^n) = 0 \quad \forall c \in \mathscr{C},\\ &F_K(\boldsymbol{U}^n_K) \geq 0,\ G_K(\boldsymbol{U}^n_K) \geq 0,\ F_K(\boldsymbol{U}^n_K)G_K(\boldsymbol{U}^n_K) = 0.\end{aligned} \tag{29}$$

Observe that system (29) is written elementwise. We define the global version of the first $2N_{\mathrm{sp}}$ lines of system (29) by

$$\mathscr{H}^n(\boldsymbol{U}^n) = 0 \quad \text{where} \quad \mathscr{H}^n : \mathbb{R}^{3N_{\mathrm{sp}}} \to \mathbb{R}^{2N_{\mathrm{sp}}} \tag{30}$$

is defined over K by the first line of (29). Inexact semismooth Newton methods will be employed to solve (29), as we detail in the next section.

4 Inexact semismooth Newton method

We detail in this section a semismooth Newton linearization associated to (29). We proceed in several steps. First, we briefly present the class of C-functions and the concept of semismoothness. Next, we give the linearization of (30) at each semismooth step.

4.1 C-functions

Definition 1 A function $f : \mathbb{R}^{N_{\rm sp}} \times \mathbb{R}^{N_{\rm sp}} \to \mathbb{R}^{N_{\rm sp}}$ is a complementarity function or (C-function) if $\forall (\boldsymbol{a}, \boldsymbol{b}) \in \mathbb{R}^{N_{\rm sp}} \times \mathbb{R}^{N_{\rm sp}}$

$$f(\boldsymbol{a}, \boldsymbol{b}) = 0 \quad \Longleftrightarrow \quad \boldsymbol{a} \geq 0, \quad \boldsymbol{b} \geq 0, \quad \boldsymbol{a}^T \boldsymbol{b} = 0.$$

Examples of C-functions are the minimum (min) function

$$(\min\{\boldsymbol{a}, \boldsymbol{b}\})_l = \min\{\boldsymbol{a}_l, \boldsymbol{b}_l\} \quad l = 1, \ldots, N_{\rm sp}, \tag{31}$$

and the Fischer–Burmeister function

$$(f_{\rm FB}(\boldsymbol{a}, \boldsymbol{b}))_l = \sqrt{\boldsymbol{a}_l^2 + \boldsymbol{b}_l^2} - (\boldsymbol{a}_l + \boldsymbol{b}_l) \quad l = 1, \ldots, N_{\rm sp}. \tag{32}$$

For a direct application of the min function, see [12, 26], and for more general details on C-functions, see [37, 38]. For $1 \leq n \leq N_t$ let C^n be any C-function satisfying

$$\begin{aligned} &C^n\left(\left(F_K(\boldsymbol{U}_K^n)\right)_{K\in\mathscr{T}_h}, \left(G_K(\boldsymbol{U}_K^n)\right)_{K\in\mathscr{T}_h}\right) = 0 \\ &\Longleftrightarrow \; F_K(\boldsymbol{U}_K^n) \geq 0, \; G_K(\boldsymbol{U}_K^n) \geq 0, \; F_K(\boldsymbol{U}_K^n) G_K(\boldsymbol{U}_K^n) = 0 \\ &\forall K \in \mathscr{T}_h. \end{aligned}$$

Introducing the function $\mathscr{C}^n : \mathbb{R}^{3N_{\rm sp}} \to \mathbb{R}^{N_{\rm sp}}$ defined as

$$\mathscr{C}^n(\boldsymbol{U}^n) = C^n\left(\left(F_K(\boldsymbol{U}_K^n)\right)_{K\in\mathscr{T}_h}, \left(G_K(\boldsymbol{U}_K^n)\right)_{K\in\mathscr{T}_h}\right), \tag{33}$$

problem (29) then reads, for all $1 \leq n \leq N_t$

$$\begin{aligned} \mathscr{H}^n(\boldsymbol{U}^n) &= 0, \\ \mathscr{C}^n(\boldsymbol{U}^n) &= 0. \end{aligned} \tag{34}$$

The disadvantage of introducing the C-function is that the problem would no longer be $\mathscr{C}^1$, thus causing problems for the local quadratic convergence of the Newton algorithm. Nevertheless, the C-functions that are commonly used are locally Lipschitz and continuous, thus differentiable almost everywhere as a result of the Rademacher Theorem (see [24, 37]). More precisely they belong to the class of strong semismooth functions. Then, it is possible (see [12, 13, 37, 38]) to build a semismooth Newton scheme.

4.2 Inexact semismooth Newton method

For $1 \leq n \leq N_t$ and $\boldsymbol{U}^{n,0} \in \mathbb{R}^{3N_{\rm sp}}$ fixed (typically $\boldsymbol{U}^{n,0} = \boldsymbol{U}^{n-1}$), the semismooth Newton algorithm generates a sequence $(\boldsymbol{U}^{n,k})_{k\geq 1}$, with $\boldsymbol{U}^{n,k} \in \mathbb{R}^{3N_{\rm sp}}$ given by the system of linear algebraic equations:

$$\mathbb{A}^{n,k-1}\boldsymbol{U}^{n,k} = \boldsymbol{B}^{n,k-1}, \tag{35}$$

where the Jacobian matrix $\mathbb{A}^{n,k-1} \in \mathbb{R}^{3N_{\rm sp},3N_{\rm sp}}$ and the right hand side vector $\boldsymbol{B}^{n,k-1} \in \mathbb{R}^{3N_{\rm sp}}$ are defined by

$$\mathbb{A}^{n,k-1} := \begin{bmatrix} \mathbf{J}_{\mathscr{H}^n}(\boldsymbol{U}^{n,k-1}) \\ \mathbf{J}_{\mathscr{C}^n}(\boldsymbol{U}^{n,k-1}) \end{bmatrix}, \tag{36}$$

$$\boldsymbol{B}^{n,k-1} := \begin{bmatrix} \mathbf{J}_{\mathscr{H}^n}(\boldsymbol{U}^{n,k-1})\boldsymbol{U}^{n,k-1} - \mathscr{H}^n(\boldsymbol{U}^{n,k-1}) \\ \mathbf{J}_{\mathscr{C}^n}(\boldsymbol{U}^{n,k-1})\boldsymbol{U}^{n,k-1} - \mathscr{C}^n(\boldsymbol{U}^{n,k-1}) \end{bmatrix}. \tag{37}$$

Note that here the $3N_{\rm sp}$ lines of (28) are nonlinear and the semismooth nonlinearity occurs in the last $N_{\rm sp}$ lines.

Here $\mathbf{J}_{\mathscr{H}^n}(\boldsymbol{U}^{n,k-1})$ is the Jacobian matrix of the function $\mathscr{H}^n$ at point $\boldsymbol{U}^{n,k-1}$ obtained by a Newton linearization and $\mathbf{J}_{\mathscr{C}^n}(\boldsymbol{U}^{n,k-1})$ is the Jacobian matrix of the semismooth function "in the sense of Clarke" (see [12, 13, 24, 37, 38]). For example, if we consider the semismooth function min of (31) and if we denote by $\boldsymbol{Y}$ the vector whose each component is defined by $\boldsymbol{Y}_l := H P'_{\rm cp}(S_{K_l}^{n,k-1})$ for $1 \leq l \leq N_{\rm sp}$ and if we define by $\mathbb{K}$ and $\mathbb{L}$ the matrices by

$$\mathbb{K} := \left[-\mathbf{Id}_{N_{\rm sp}\times N_{\rm sp}}, \mathbf{0}_{N_{\rm sp}\times N_{\rm sp}}, \mathbf{0}_{N_{\rm sp}\times N_{\rm sp}}\right],$$

$$\mathbb{L} := \left[\mathrm{diag}\boldsymbol{Y}_{N_{\rm sp}\times N_{\rm sp}}, H \times \mathbf{Id}_{N_{\rm sp}\times N_{\rm sp}}, -\beta^1 \times \mathbf{Id}_{N_{\rm sp}\times N_{\rm sp}}\right],$$

then, the lth row of the matrix $\mathbf{J}_{\mathscr{C}^n}(\boldsymbol{U}^{n,k-1})$ is either given by the lth row of $\mathbb{K}$ if

$$1 - S_{K_l}^{n,k-1} \leq H\left[P_{K_l}^{n,k-1} + P_{\rm cp}(S_{K_l}^{n,k-1})\right] - \beta^1 \chi_{K_l}^{n,k-1},$$

or by the lth line of $\mathbb{L}$ if

$$H\left[P_{K_l}^{n,k-1} + P_{\rm cp}(S_{K_l}^{n,k-1})\right] - \beta^1 \chi_{K_l}^{n,k-1} < 1 - S_{K_l}^{n,k-1}.$$

Next, the approximate solution to (35) is obtained using an iterative algebraic solver. For $1 \leq n \leq N_t$, a fixed semismooth Newton step $k \geq 1$, and an initial guess $\boldsymbol{U}^{n,k,0}$ (usually, $\boldsymbol{U}^{n,k,0} = \boldsymbol{U}^{n,k-1}$) the iterative algebraic solver generates a sequence $(\boldsymbol{U}^{n,k,i})_{i\geq 0}$ satisfying

$$\mathbb{A}^{n,k-1}\boldsymbol{U}^{n,k,i} = \boldsymbol{B}^{n,k-1} - \boldsymbol{R}^{n,k,i} \tag{38}$$

where $\boldsymbol{R}^{n,k,i} \in \mathbb{R}^{3N_{\rm sp}}$ is the algebraic residual vector. Below, it will be convenient to use the detailed form of the first two equations of (38):

$$\begin{aligned} &\frac{|K|}{\tau_n}\left[l_{c,K}\left(\boldsymbol{U}^{n,k-1}\right) - l_{c,K}^{n-1} + \mathscr{L}_{c,K}^{n,k,i}\right] + \sum_{\sigma\in\mathscr{E}_K^{\rm int}} \mathscr{F}_{c,K,\sigma}^{n,k,i} \\ &-|K| Q_{c,K}^n + \boldsymbol{R}_{c,K}^{n,k,i} = 0, \quad \forall K \in \mathscr{T}_h \end{aligned} \tag{39}$$

with the linear perturbation in the accumulation defined by

$$\mathscr{L}_{c,K}^{n,k,i} := \sum_{K' \in \mathscr{T}_h} \frac{\partial l_{c,K}^{n}}{\partial \boldsymbol{U}_{K'}}(\boldsymbol{U}^{n,k-1}) \left[\boldsymbol{U}_{K'}^{n,k,i} - \boldsymbol{U}_{K'}^{n,k-1} \right],$$

and the linearized component flux by

$$\mathscr{F}_{c,K,\sigma}^{n,k,i} := \sum_{K' \in \mathscr{T}_h} \frac{\partial F_{c,K,\sigma}}{\partial \boldsymbol{U}_{K'}} \left(\boldsymbol{U}^{n,k-1} \right) \left[\boldsymbol{U}_{K'}^{n,k,i} - \boldsymbol{U}_{K'}^{n,k-1} \right] + F_{c,K,\sigma} \left(\boldsymbol{U}^{n,k-1} \right). \tag{40}$$

5 A posteriori error estimates

5.1 Preamble

In this section, we establish an a posteriori error estimate between the exact solution and its approximate numerical solution at each semismooth Newton step $k \geq 1$ and each linear algebraic step $i \geq 0$. We start by giving some additional generic notations. Concerning the discrete unknowns, as we employed the cell-centered finite volume method, for each time step $0 \leq n \leq N_t$ and for each $k \geq 1$ and $i \geq 0$, the discrete liquid pressure as well as the discrete liquid saturation and the discrete molar fraction of liquid hydrogen are piecewise constant in space. To carry out properly the a posteriori analysis, the discrete pressures and the discrete molar fraction of liquid hydrogen should belong to $H^1(\Omega)$ which is not the case. Therefore we assume that, from the constant finite volume unknowns, we have constructed discontinuous piecewise quadratic-in-space functions $P_h^{n,k,i} \in \mathbb{P}_2^{\mathrm{d}}(\mathscr{T}_h)$ (liquid pressure), $\chi_h^{n,k,i} \in \mathbb{P}_2^{\mathrm{d}}(\mathscr{T}_h)$ (molar fraction). We will also employ continuous piecewise quadratic functions $\tilde{P}_h^{n,k,i} \in \mathbb{P}_2^{\mathrm{c}}(\mathscr{T}_h)$, and $\tilde{\chi}_h^{n,k,i} \in \mathbb{P}_2^{\mathrm{c}}(\mathscr{T}_h)$. As an intermediate of computation we will also need to construct a discontinuous piecewise quadratic-in-space gas pressure function $P_h^{\mathrm{g},n,k,i}$ (see Section 5.3). The saturation and thus the amount of water and hydrogen are defined in $\mathbb{P}_0^{\mathrm{d}}(\mathscr{T}_h)$ by

$$S_h^{n,k,i}|_K(\boldsymbol{x}) = S_K^{n,k,i}, \quad l_{\mathrm{w},h}^{n,k,i}|_K(\boldsymbol{x}) = l_{\mathrm{w},K}^{n,k,i}, \quad l_{\mathrm{h},h}^{n,k,i}|_K = l_{\mathrm{h},K}^{n,k,i}, \quad \forall K \in \mathscr{T}_h. \tag{41}$$

From the above space functions, we define the space-time functions as continuous and piecewise affine in time (i.e., in $\mathbb{P}_1^{\mathrm{c}}(0, t_{\mathrm{F}})$) by

$$P_{h\tau}^{n,k,i}(t^n) = P_h^{n,k,i},\ \tilde{P}_{h\tau}^{n,k,i}(t^n) = \tilde{P}_h^{n,k,i},\ l_{c,h\tau}^{n,k,i}(t^n) = l_{c,h}^{n,k,i},$$
$$S_{h\tau}^{n,k,i}(t^n) = S_h^{n,k,i},\ \chi_{h\tau}^{n,k,i}(t^n) = \chi_h^{n,k,i},\ \tilde{\chi}_{h\tau}^{n,k,i}(t^n) = \tilde{\chi}_h^{n,k,i}. \tag{42}$$

Concerning the source terms, we define the space-time function $Q_{c,h\tau}$ such that $\left(Q_{c,h\tau}\right)|_{K\times I_n} = Q_{c,K}^n$, thus piecewise constant in time and in space. To finish we assume that the initial condition (18) holds. For the a posteriori analysis, the goal would be to find an upper bound of the form:

$$\left\| P^{\mathrm{l}} - P_{h\tau}^{n,k,i} \right\|_\sharp + \left\| S^{\mathrm{l}} - S_{h\tau}^{n,k,i} \right\|_\sharp + \left\| \chi_{\mathrm{h}}^{\mathrm{l}} - \chi_{h\tau}^{n,k,i} \right\|_\sharp \leq \eta,$$

with $\|\cdot\|_\sharp$ some norm and η only depending on the approximate solution. This kind of estimate has to our knowledge not been established for compositional multiphase flow. In the literature, such an a posteriori error estimate has been derived for a two-phase flow with one component per phase (see [17]). We thus follow the methodology proposed in [29, 72] by considering some dual norm of the residual. We first start by defining appropriate spaces for the unknowns. Let X, Y, $\widehat{Y}$, and Z be the spaces defined by:

$$X := L^2((0, t_{\mathrm{F}}); H^1(\Omega)),$$
$$Y := H^1((0, t_{\mathrm{F}}); L^2(\Omega)),$$
$$\widehat{Y} := H^1((0, t_{\mathrm{F}}); L^\infty(\Omega)),$$
$$Z := \left\{ v \in L^2((0, t_{\mathrm{F}}); L^\infty(\Omega)),\ v \geq 0 \text{ on } \Omega \times (0, t_{\mathrm{F}}) \right\}.$$

We denote by X_n the restriction of the energy space X to the time interval I_n, $X_n := L^2\left(I_n; H^1(\Omega)\right)$. We equip the spaces X and X_n with the norms

$$\|\varphi\|_X := \left\{ \sum_{n=1}^{N_t} \|\varphi\|_{X_n}^2 \, \mathrm{dt} \right\}^{\frac{1}{2}}, \quad \|\varphi\|_{X_n} := \left\{ \int_{I_n} \sum_{K \in \mathscr{T}_h} \|\varphi\|_{X,K}^2 \, \mathrm{dt} \right\}^{\frac{1}{2}}, \tag{43}$$

with $\|\varphi\|_{X,K}^2 := \varepsilon h_K^{-2} \|\varphi\|_K^2 + \|\nabla\varphi\|_K^2$.

Note that $\varepsilon = 0$ is to be chosen when homogeneous Dirichlet conditions are prescribed on the boundary $\partial\Omega$, whereas $\varepsilon > 0$ enables to take into account Neumann boundary conditions. Then, h_K^{-2} is a scaling term.

5.2 Weak solution

Let $Q_c \in L^2((0, t_{\mathrm{F}}); L^2(\Omega))\ \forall c \in \mathscr{C}$. We assume that there exists a unique weak solution satisfying:

Assumption 2

$$S^{\mathrm{l}} \in \widehat{Y}, \quad 1 - S^{\mathrm{l}} \in Z, \quad l_{\mathrm{w}} \in Y, \quad l_{\mathrm{h}} \in Y, \tag{44}$$

$$P^{\mathrm{l}} \in X, \quad \chi_{\mathrm{h}}^{\mathrm{l}} \in X, \tag{45}$$

$$\boldsymbol{\Phi}_c \in [L^2((0,t_\mathrm{F});\mathbf{H}(\mathrm{div},\Omega)]^2 \quad \forall c \in \mathscr{C}, \tag{46}$$

$$\int_0^{t_\mathrm{F}} (\partial_t l_c, \varphi)_\Omega(t)\,\mathrm{dt} - \int_0^{t_\mathrm{F}} (\boldsymbol{\Phi}_c, \nabla\varphi)_\Omega(t)\,\mathrm{dt} = \int_0^{t_\mathrm{F}} (Q_c,\varphi)_\Omega(t)\,\mathrm{dt} \quad \forall \varphi \in X \quad \forall c \in \mathscr{C}, \tag{47}$$

$$\int_0^{t_\mathrm{F}} \left(\lambda - \left(1-S^\mathrm{l}\right), H[P^\mathrm{l}+P_\mathrm{cp}(S^\mathrm{l})] - \beta^\mathrm{l}\chi_\mathrm{h}^\mathrm{l}\right)_\Omega(t)\,\mathrm{dt} \geq 0 \quad \forall \lambda \in Z, \tag{48}$$

and the initial condition (18) *holds, where* l_c *and* $\boldsymbol{\Phi}_c$ *are defined by* (17), (15), *and* (16).

Remark 1 In Assumption 2, we characterize the weak solution for the continuous two-phase problem with phase transition (14) and suppose that it exists and is unique. Under this assumption, we can define below an error measure for the error between the weak and approximate solutions. We are not aware of affirmative existence and uniqueness results for the phase transition problem (14). For the simpler two-phase flow model with one component per phase and no phase transition, it is possible to prove existence and uniqueness of the weak solution under specific assumptions on the unknowns and parameters of the model (see [3], [4], [49], and [19]). In [17], an a posteriori error estimate for a two-phase flow model with weak solution based the global pressure is established. This result states that an energy-type norm of the differences between the exact and the approximate nonwetting phase saturations and the global pressures and its discrete analogue can be bounded first by a dual residual norm (cf. (51) and (52)) by a fully computable a posteriori error estimate.

Proposition 1 *Under assumption* (44), *the nonlinear complementarity conditions given by the third line of* (14) *are equivalent to the assumption* (48).

Proof Suppose that the third line of the strong formulation (14) holds. Let $\lambda \in Z$. We have $1 - S^\mathrm{l} \in Z$ and

$$\int_0^{t_\mathrm{F}} \left(\lambda - \left(1-S^\mathrm{l}\right), H[P^\mathrm{l}+P_\mathrm{cp}(S^\mathrm{l})] - \beta^\mathrm{l}\chi_\mathrm{h}^\mathrm{l}\right)_\Omega(t)\,\mathrm{dt} = \int_0^{t_\mathrm{F}} \left(\lambda, H\left[P^\mathrm{l}+P_\mathrm{cp}(S^\mathrm{l})\right] - \beta^\mathrm{l}\chi_\mathrm{h}^\mathrm{l}\right)_\Omega(t)\,\mathrm{dt} \geq 0.$$

Conversely, suppose that the assumption (48) is satisfied.

For $\lambda = 0 \in Z$ we have

$$\int_0^{t_\mathrm{F}} \left(1 - S^\mathrm{l}, H[P^\mathrm{l}+P_\mathrm{cp}(S^\mathrm{l})] - \beta^\mathrm{l}\chi_\mathrm{h}^\mathrm{l}\right)_\Omega(t)\,\mathrm{dt} \leq 0. \tag{49}$$

Next, for $\lambda(x,t) = 1 - S^\mathrm{l}(x,t) + \mathbb{1}_{\mathscr{O}\times[t-\zeta,t+\zeta]}$ where $\zeta > 0$ and $\mathscr{O}$ is any measurable subset of Ω we have $\lambda \in Z$ as $1 - S^\mathrm{l} \in Z$; thus

$$H[P^\mathrm{l}(x,t) + P_\mathrm{cp}(S^\mathrm{l}(x,t))] - \beta^\mathrm{l}\chi_\mathrm{h}^\mathrm{l}(x,t) \geq 0. \tag{50}$$

Therefore, combining (49), (50), and the assumption $1 - S^\mathrm{l} \geq 0$, we get

$$\left[1 - S^\mathrm{l}\right]\left[H\left[P^\mathrm{l} + P_\mathrm{cp}(S^\mathrm{l})\right] - \beta^\mathrm{l}\chi_\mathrm{h}^\mathrm{l}\right] = 0.$$

□

5.3 Error measure

As discussed in Section 5.1, the natural choice is to consider an error measure constructed from the dual norm of a residual supplemented by the nonconformity of the liquid pressure and the molar fraction of liquid hydrogen following [29] and the references therein. As we treat the phase transitions, we also have to add a term checking the complementarity constraints.

Definition 2 For the discrete approximations $P_{h\tau}^{n,k,i}$ and $\chi_{h\tau}^{n,k,i}$ belonging to $L^2(I_n; H^1(\mathscr{T}_h))$ to be defined later in Section 5.5 and $S_{h\tau}^{n,k,i}$ given by (41)–(42), the residual associated to assumption (47) is defined for any $\varphi \in X_n$ by

$$\langle \mathscr{R}_c(S_{h\tau}^{n,k,i}, P_{h\tau}^{n,k,i}, \chi_{h\tau}^{n,k,i}), \varphi\rangle_{X_n',X_n} := \int_{I_n} \left\{\left(Q_c - \partial_t l_{c,h\tau}^{n,k,i}, \varphi\right)_\Omega + \left(\boldsymbol{\Phi}_{c,h\tau}^{n,k,i}, \nabla\varphi\right)_\Omega\right\}(t)\,\mathrm{dt}, \tag{51}$$

and its dual norm is defined by

$$\left\|\mathscr{R}_c(S_{h\tau}^{n,k,i}, P_{h\tau}^{n,k,i}, \chi_{h\tau}^{n,k,i})\right\|_{X_n'} := \sup_{\varphi\in X_n, \|\varphi\|_{X_n}=1} \langle \mathscr{R}_c(S_{h\tau}^{n,k,i}, P_{h\tau}^{n,k,i}, \chi_{h\tau}^{n,k,i}), \varphi\rangle_{X_n',X_n}, \tag{52}$$

where $\boldsymbol{\Phi}_{c,h\tau}^{n,k,i}$, $c \in \mathscr{C}$, are the discrete fluxes corresponding to (15) and (16) defined by

$$\boldsymbol{\Phi}_{\mathrm{w},h\tau}^{n,k,i} := \rho_\mathrm{w}^\mathrm{l}\mathbf{q}_{h\tau}^{n,k,i} - \mathbf{J}_{\mathrm{h},h\tau}^{n,k,i},$$

$$\boldsymbol{\Phi}_{\mathrm{h},h\tau}^{n,k,i} := \beta^\mathrm{l}\chi_{h\tau}^{n,k,i}\mathbf{q}_{h\tau}^{n,k,i} + \beta^\mathrm{g}\left[P_\mathrm{cp}(S_{h\tau}^{n,k,i}) + P_{h\tau}^{n,k,i}\right]\mathbf{q}_{h\tau}^{\mathrm{g},n,k,i} + \mathbf{J}_{\mathrm{h},h\tau}^{n,k,i},$$

where the discrete Darcy space-time vectorial functions $\mathbf{q}_{h\tau}^{n,k,i}$ and $\mathbf{q}_{h\tau}^{\mathrm{g},n,k,i}$ and the discrete liquid Fick space-time vectorial function $\mathbf{J}_{\mathrm{h},h\tau}^{n,k,i}$ are defined by

$$\begin{aligned}
\mathbf{q}_{h\tau}^{n,k,i} &:= -\underline{\mathbf{K}}\frac{k_{\mathrm{r}}^{\mathrm{l}}(S_{h\tau}^{n,k,i})}{\mu^{\mathrm{l}}}\Big[\nabla P_{h\tau}^{n,k,i} - \Big[\rho_{\mathrm{w}}^{\mathrm{l}} + \beta^{\mathrm{l}}\chi_{h\tau}^{n,k,i}\Big] g\nabla z\Big],\\
\mathbf{q}_{h\tau}^{\mathrm{g},n,k,i} &:= -\underline{\mathbf{K}}\frac{k_{\mathrm{r}}^{\mathrm{g}}(1-S_{h\tau}^{n,k,i})}{\mu^{\mathrm{g}}}\Big[\nabla P_{h\tau}^{\mathrm{g},n,k,i} - \beta^{\mathrm{g}} P_{h\tau}^{\mathrm{g},n,k,i} g\nabla z\Big],\\
\mathbf{J}_{\mathrm{h},h\tau}^{n,k,i} &:= -\phi M_{\mathrm{h}} S_{h\tau}^{n,k,i}\left[\frac{\rho_{\mathrm{w}}^{\mathrm{l}}}{M_{\mathrm{w}}} + \frac{\beta^{\mathrm{l}}}{M_{\mathrm{h}}}\chi_{h\tau}^{n,k,i}\right] D_{\mathrm{h}}^{\mathrm{l}}\nabla\chi_{h\tau}^{n,k,i},
\end{aligned}$$

where the space-time function $P_{h\tau}^{\mathrm{g},n,k,i}$ is built from $P_{h\tau}^{n,k,i}$ and $S_{h\tau}^{n,k,i}$ in Section 5.5 below. Furthermore, we define the residual equation associated to assumption (48) as

$$\begin{aligned}
&\mathscr{R}_{\mathrm{e}}(S_{h\tau}^{n,k,i}, P_{h\tau}^{n,k,i}, \chi_{h\tau}^{n,k,i})\\
&:= \frac{1}{\alpha}\times\left[\int_{I_n}\Big(1-S_{h\tau}^{n,k,i}, H\Big[P_{h\tau}^{n,k,i}+P_{\mathrm{cp}}(S_{h\tau}^{n,k,i})\Big]-\beta^{\mathrm{l}}\chi_{h\tau}^{n,k,i}\Big)_{\Omega}(t)\,\mathrm{d}t\right],
\end{aligned}$$

with $\alpha > 0$ a rescaling constant.

We define our error measure by

$$\begin{aligned}
\mathscr{N}^{n,k,i} &:= \left\{\sum_{c\in\mathscr{C}}\left\|\mathscr{R}_c(S_{h\tau}^{n,k,i}, P_{h\tau}^{n,k,i}, \chi_{h\tau}^{n,k,i})\right\|_{X_n'}^2\right\}^{\frac{1}{2}}\\
&\quad+\left\{\Big[\mathscr{N}_P^{n,k,i}(P_{h\tau}^{n,k,i})\Big]^2+\Big[\mathscr{N}_\chi^{n,k,i}(\chi_{h\tau}^{n,k,i})\Big]^2\right\}^{\frac{1}{2}}\\
&\quad+\mathscr{R}_{\mathrm{e}}(S_{h\tau}^{n,k,i}, P_{h\tau}^{n,k,i}, \chi_{h\tau}^{n,k,i}),
\end{aligned}\tag{53}$$

with

$$\begin{aligned}
\mathscr{N}_P^{n,k,i}(P_{h\tau}^{n,k,i}) &:= \inf_{\delta_{\mathrm{l}}\in X_n}\left\{\sum_{c\in\mathscr{C}^{\mathrm{l}}}\int_{I_n}\right.\\
&\qquad\left.\left\|\boldsymbol{\Upsilon}_{\mathrm{l},c}(P_{h\tau}^{n,k,i})(t)-\boldsymbol{\Upsilon}_{\mathrm{l},c}(\delta_{\mathrm{l}})(t)\right\|^2\mathrm{d}t\right\}^{\frac{1}{2}},
\end{aligned}\tag{54}$$

$$\begin{aligned}
\mathscr{N}_\chi^{n,k,i}(\chi_{h\tau}^{n,k,i}) &:= \inf_{\theta\in X_n}\left\{\int_{I_n}\right.\\
&\qquad\left.\left\|\boldsymbol{\Psi}(\chi_{h\tau}^{n,k,i})(t)-\boldsymbol{\Psi}(\theta)(t)\right\|^2\mathrm{d}t\right\}^{\frac{1}{2}},
\end{aligned}\tag{55}$$

where the function $\boldsymbol{\Upsilon}_{\mathrm{l},c}$ is defined by

$$\begin{aligned}
\boldsymbol{\Upsilon}_{\mathrm{l,w}}(\varphi) &:= -\underline{\mathbf{K}}\frac{k_{\mathrm{r}}^{\mathrm{l}}(S_{h\tau}^{n,k,i})}{\mu^{\mathrm{l}}}\rho_{\mathrm{w}}^{\mathrm{l}}\nabla\varphi,\\
\boldsymbol{\Upsilon}_{\mathrm{l,h}}(\varphi) &:= -\underline{\mathbf{K}}\frac{k_{\mathrm{r}}^{\mathrm{l}}(S_{h\tau}^{n,k,i})}{\mu^{\mathrm{l}}}\beta^{\mathrm{l}}\chi_{\mathrm{h}}^{\mathrm{l}}\nabla\varphi,\\
&\quad\forall\varphi\in L^2(I_n; H^1(\mathscr{T}_h))
\end{aligned}$$

and the function $\boldsymbol{\Psi}$ defined by

$$\begin{aligned}
\boldsymbol{\Psi}(\varphi) &:= -\phi M_{\mathrm{h}} S_{h\tau}^{n,k,i}\left[\frac{\rho_{\mathrm{w}}^{\mathrm{l}}}{M_{\mathrm{w}}}+\frac{\beta^{\mathrm{l}}}{M_{\mathrm{h}}}\chi_{h\tau}^{n,k,i}\right] D_{\mathrm{h}}^{\mathrm{l}}\nabla\varphi,\\
&\forall\varphi\in L^2(I_n; H^1(\mathscr{T}_h)).
\end{aligned}$$

5.4 Equilibrated component flux reconstructions

Let $1 \le n \le N_t$, a semismooth Newton linearization iteration $k \ge 1$, and an algebraic solver iteration $i \ge 0$ be fixed. We are interested in finding an upper bound for the error measure $\mathscr{N}^{n,k,i}$ defined in (53). To do so, we employ the methodology of the equilibrated flux reconstruction in the context of the cell-centered finite volume method [29, 30, 32]. The subspace of $\mathbf{H}(\mathrm{div}, \Omega)$ we use in the sequel is the lowest order Raviart–Thomas space (see Raviart and Thomas [63], or Roberts and Thomas [66], or Brezzi and Fortin [16]) and is defined by

$$\begin{aligned}
&\mathbf{RT}_0(\Omega) := \{\boldsymbol{w}_h\in\mathbf{H}(\mathrm{div},\Omega),\ \boldsymbol{w}_h|_K\in\mathbf{RT}_0(K)\ \forall K\in\mathscr{T}_h\},\\
&\mathbf{RT}_0(K) := [\mathbb{P}_0(K)]^2 + x\cdot\mathbb{P}_0(K) \text{ with } x = \begin{pmatrix} x\\ y\end{pmatrix}.
\end{aligned}$$

For a function $\boldsymbol{v}\in\mathbf{RT}_0(K)$, we recall that its 3 degrees of freedom are given by $(\boldsymbol{v}\cdot\boldsymbol{n}_{K,\sigma}, 1)_\sigma, \sigma\in\mathscr{E}_K$.
For all component $c\in\mathscr{C}$, for all $K\in\mathscr{T}_h$, and for all $\sigma\in\mathscr{E}_K^{\mathrm{int}}$ we can define from (20), (26), and (39) the different component flux reconstructions in $\mathbf{RT}_0(\mathscr{T}_h)$, namely the discretization flux reconstruction $\boldsymbol{\Theta}_{c,h,\mathrm{disc}}^{n,k,i}$, the linearization flux reconstruction $\boldsymbol{\Theta}_{c,h,\mathrm{lin}}^{n,k,i}$, and the algebraic flux reconstruction $\boldsymbol{\Theta}_{c,h,\mathrm{alg}}^{n,k,i}$ as follows

$$\left(\boldsymbol{\Theta}_{c,h,\mathrm{disc}}^{n,k,i}\cdot\boldsymbol{n}_{K,\sigma}, 1\right)_\sigma := F_{c,K,\sigma}\left(\boldsymbol{U}^{n,k,i}\right),\tag{56}$$

$$\left(\boldsymbol{\Theta}_{c,h,\mathrm{lin}}^{n,k,i}\cdot\boldsymbol{n}_{K,\sigma}, 1\right)_\sigma := \mathscr{F}_{c,K,\sigma}^{n,k,i} - F_{c,K,\sigma}\left(\boldsymbol{U}^{n,k,i}\right),\tag{57}$$

$$\boldsymbol{\Theta}_{c,h,\mathrm{alg}}^{n,k,i,\nu} := \boldsymbol{\Theta}_{c,h,\mathrm{disc}}^{n,k,i+\nu} + \boldsymbol{\Theta}_{c,h,\mathrm{lin}}^{n,k,i+\nu} - \left(\boldsymbol{\Theta}_{c,h,\mathrm{disc}}^{n,k,i} + \boldsymbol{\Theta}_{c,h,\mathrm{lin}}^{n,k,i}\right)\tag{58}$$

with a fixed number $\nu > 0$ of additional algebraic iterations.

Here $F_{c,K,\sigma}$ is defined by (21) or (27), and $\mathscr{F}_{c,K,\sigma}^{n,k,i}$ is defined by (40). For the boundary conditions, we set $\boldsymbol{\Theta}_{c,h,\mathrm{disc}}^{n,k,i}\cdot\boldsymbol{n}_{K,\sigma} = \boldsymbol{\Theta}_{c,h,\mathrm{lin}}^{n,k,i}\cdot\boldsymbol{n}_{K,\sigma} = \boldsymbol{\Theta}_{c,h,\mathrm{alg}}^{n,k,i,\nu}\cdot\boldsymbol{n}_{K,\sigma} = 0$ for $\sigma\in\mathscr{E}_h^{\mathrm{ext}}$. Therefrom, we define $\forall c\in\mathscr{C}$, the total flux reconstruction $\boldsymbol{\Theta}_{c,h}^{n,k,i,\nu}$ by

$$\boldsymbol{\Theta}_{c,h}^{n,k,i,\nu} := \boldsymbol{\Theta}_{c,h,\mathrm{disc}}^{n,k,i} + \boldsymbol{\Theta}_{c,h,\mathrm{lin}}^{n,k,i} + \boldsymbol{\Theta}_{c,h,\mathrm{alg}}^{n,k,i,\nu}.\tag{59}$$

Remark 2 The component fluxes $\boldsymbol{\Theta}_{c,h,\mathrm{disc}}^{n,k,i}$, $\boldsymbol{\Theta}_{c,h,\mathrm{lin}}^{n,k,i}$, $\boldsymbol{\Theta}_{c,h,\mathrm{alg}}^{n,k,i,\nu}$ belong to $\mathbf{H}(\mathrm{div}, \Omega)$.

Note that it is possible in practice to change the definition (58) (see [58] for a reconstruction based on a multigrid structure).

We have,

Proposition 2 *Let $1 \leq n \leq N_t$, a semismooth Newton iteration $k \geq 1$, and an algebraic solver iteration $i \geq 0$ be fixed and $\nu > 0$. For all $c \in \mathscr{C}$ and for all $K \in \mathscr{T}_h$ there holds,*

$$\left(Q_{c,K}^n - \frac{l_{c,K}(\boldsymbol{U}^{n,k-1}) - l_{c,K}^{n-1} + \mathscr{L}_{c,K}^{n,k,i+\nu}}{\tau_n} - \boldsymbol{\nabla}\cdot\boldsymbol{\Theta}_{c,h}^{n,k,i,\nu}, 1\right)_K = \boldsymbol{R}_{c,K}^{n,k,i+\nu}. \tag{60}$$

Proof Employing the definition of the total fluxes (59), the definition of the component fluxes (56)–(58), and the Green formula we get

$$\left(-\boldsymbol{\nabla}\cdot\boldsymbol{\Theta}_{c,h}^{n,k,i,\nu}, 1\right)_K = -\sum_{\sigma\in\mathscr{E}_K^{\rm int}} \mathscr{F}_{c,K,\sigma}^{n,k,i+\nu}.$$

Thus, equation (39) at iterate $i+\nu$ yields the desired result. □

5.5 Phase pressure and molar fraction reconstructions

We present in this section the construction from the finite volume unknowns of the discontinuous quadratic liquid pressure and molar fraction of liquid hydrogen and next their continuous quadratic interpolant so as to preserve the physical properties imposed by the problem.

Let $1 \leq n \leq N_t$, we define $\left(\boldsymbol{\xi}_h^{n,k,i}, \boldsymbol{\xi}_h^{{\rm g},n,k,i}\right) \in \mathbf{RT}_0(\mathscr{T}_h) \times \mathbf{RT}_0(\mathscr{T}_h)$ such that $\forall K \in \mathscr{T}_h$ and $\forall \sigma \in \mathscr{E}_K^{\rm int}$ such that $\overline{\sigma} = \overline{K} \cap \overline{L}$

$$\left(\boldsymbol{\xi}_h^{n,k,i}\cdot\boldsymbol{n}_{K,\sigma}, 1\right)_\sigma := -|\sigma|\frac{P_L^{n,k,i} - P_K^{n,k,i}}{d_{KL}},$$

$$\left(\boldsymbol{\xi}_h^{{\rm g},n,k,i}\cdot\boldsymbol{n}_K, 1\right)_\sigma := -|\sigma|\frac{P_L^{{\rm g},n,k,i} - P_K^{{\rm g},n,k,i}}{d_{KL}},$$

with

$$P_K^{{\rm g},n,k,i} = P_K^{n,k,i} + P_{\rm cp}(S_K^{n,k,i}).$$

The discontinuous piecewise quadratic liquid phase pressure $P_h^{n,k,i} \in \mathbb{P}_2^{\rm d}(\mathscr{T}_h)$ is such that $\forall K \in \mathscr{T}_h$

$$\left(-\boldsymbol{\nabla} P_h^{n,k,i}\right)|_K := \left(\boldsymbol{\xi}_h^{n,k,i}\right)_K \quad \text{and} \quad \frac{\left(P_h^{n,k,i}, 1\right)_K}{|K|} := P_K^{n,k,i}.$$

while the discontinuous quadratic gas phase pressure $P_h^{{\rm g},n,k,i} \in \mathbb{P}_2^{\rm d}(\mathscr{T}_h)$ satisfies $\forall K \in \mathscr{T}_h$

$$\left(-\boldsymbol{\nabla} P_h^{{\rm g},n,k,i}\right)|_K := \left(\boldsymbol{\xi}_h^{{\rm g},n,k,i}\right)_K, \text{ and } \frac{\left(P_h^{{\rm g},n,k,i}, 1\right)_K}{|K|} := P_K^{{\rm g},n,k,i}.$$

Until now, we have transformed a constant in each cells onto a discontinuous $\mathbb{P}_2$ polynomial. This transformation unfortunately does not give the global continuity in space so that $P_h^{n,k,i}$ and $P_h^{{\rm g},n,k,i}$ do not belong to $H^1(\Omega)$. To do so, we use the Oswald interpolation operator (see [46, 71]) that associates to the discontinuous piecewise polynomial $P_h^{n,k,i}$ its conforming interpolant.

Then, from $P_h^{n,k,i} \in \mathbb{P}_2^{\rm d}(\mathscr{T}_h)$, using the notations introduced at the beginning of Section 3.1, we define $\tilde{P}_h^{n,k,i} \in \mathbb{P}_2^{\rm c}(\mathscr{T}_h)$ by

$$\tilde{P}_h^{n,k,i}(\boldsymbol{a}) := \frac{1}{|\mathscr{T}_{\boldsymbol{a}}|}\sum_{K\in\mathscr{T}_{\boldsymbol{a}}}\left(P_h^{n,k,i}\right)|_K(\boldsymbol{a}) \quad \text{for} \quad \boldsymbol{a} \in D_2. \tag{61}$$

In the same way, we reconstruct a continuous $\mathbb{P}_2^{\rm c}(\mathscr{T}_h)$ molar fraction as follows. Let $1 \leq n \leq N_t$, we define $\boldsymbol{v}_h^{n,k,i} \in \mathbf{RT}_0(\mathscr{T}_h)$ such that $\forall K \in \mathscr{T}_h$ and $\forall \sigma \in \mathscr{E}_K^{\rm int}$ such that $\overline{\sigma} = \overline{K} \cap \overline{L}$,

$$\left(\boldsymbol{v}_h^{n,k,i}\cdot\boldsymbol{n}_K, 1\right)_\sigma := -|\sigma|\frac{\chi_L^{n,k,i} - \chi_K^{n,k,i}}{d_{KL}}.$$

The discontinuous quadratic molar fraction $\chi_h^{n,k,i}$ is such that $\forall K \in \mathscr{T}_h$,

$$\left(-\boldsymbol{\nabla}\chi_h^{n,k,i}\right)|_K := \left(\boldsymbol{v}_h^{n,k,i}\right)_K \quad \text{and} \quad \frac{\left(\chi_h^{n,k,i}, 1\right)_K}{|K|} := \chi_K^{n,k,i}.$$

From the discontinuous polynomial $\chi_h^{n,k,i} \in \mathbb{P}_2^{\rm d}(\mathscr{T}_h)$, we construct its conforming interpolant, using the Oswald interpolation operator as follows

$$\tilde{\chi}_h^{n,k,i}(\boldsymbol{a}) := \frac{1}{|\mathscr{T}_{\boldsymbol{a}}|}\sum_{K\in\mathscr{T}_{\boldsymbol{a}}}\left(\chi_h^{n,k,i}\right)|_K(\boldsymbol{a}) \quad \boldsymbol{a} \in D_2. \tag{62}$$

Remark 3 The constructions (61) and (62) give $\tilde{P}_h^{n,k,i}$ and $\tilde{\chi}_h^{n,k,i} \in H^1(\Omega)$.

5.6 A posteriori error estimates

In this section we provide an upper bound for the error measure defined in (53) at each semismooth step $k \geq 1$ and each algebraic iteration $i \geq 0$. An important difficulty is that during the iterations in i and k, the approximation is no more conforming in the sense that the conditions

$$1 - S_{h\tau}^{n,k,i} \geq 0, \quad H\left[P_{h\tau}^{n,k,i} + P_{\rm cp}(S_{h\tau}^{n,k,i})\right] - \beta^{\rm l}\chi_{h\tau}^{n,k,i} \geq 0,$$
$$\left[1 - S_{h\tau}^{n,k,i}\right]\left[H\left[P_{h\tau}^{n,k,i} + P_{\rm cp}(S_{h\tau}^{n,k,i})\right] - \beta^{\rm l}\chi_{h\tau}^{n,k,i}\right] = 0$$

do not necessarily hold.

We define for all $c \in \mathscr{C}$ the estimators linked to the finite volume discretization

$$\eta_{\mathrm{R},K,c}^{n,k,i,\nu} := \min\left\{C_{\mathrm{PW}}, \varepsilon^{-\frac{1}{2}}\right\} h_K \left\| Q_{c,K}^n - \frac{1}{\tau_n} \times \left[l_{c,K}(\boldsymbol{U}^{n,k-1}) - l_{c,K}^{n-1} + \mathscr{L}_{c,K}^{n,k,i+\nu} \right] - \frac{\boldsymbol{R}_{c,K}^{n,k,i+\nu}}{|K|} - \nabla \cdot \boldsymbol{\Theta}_{c,h}^{n,k,i,\nu} \right\|_K, \tag{63}$$

$$\eta_{\mathrm{F},K,c}^{n,k,i,\nu}(t) := \left\| \boldsymbol{\Theta}_{c,h}^{n,k,i,\nu} - \boldsymbol{\Phi}_{c,h\tau}^{n,k,i}(t) \right\|_K \quad t \in I_n, \tag{64}$$

the estimators linked to the nonconformity of the liquid pressure and the molar fraction of liquid hydrogen

$$\eta_{\mathrm{NC},K,1,c}^{n,k,i}(t) := \left\| \boldsymbol{\Upsilon}_{1,c}(P_{h\tau}^{n,k,i})(t) - \boldsymbol{\Upsilon}_{1,c}(\tilde{P}_{h\tau}^{n,k,i})(t) \right\|_K \quad t \in I_n,\ c \in \mathscr{C}, \tag{65}$$

$$\eta_{\mathrm{NC},K,\chi}^{n,k,i}(t) := \left\| \boldsymbol{\Psi}(\chi_{h\tau}^{n,k,i})(t) - \boldsymbol{\Psi}(\tilde{\chi}_{h\tau}^{n,k,i})(t) \right\|_K \quad t \in I_n, \tag{66}$$

and the estimators linked respectively to the semismooth linearization and linear algebra

$$\eta_{\mathrm{NA},K,c}^{n,k,i,\nu} := \varepsilon^{-\frac{1}{2}} \frac{h_K}{\tau_n} \times \left\| l_{c,K}(\boldsymbol{U}^{n,k,i}) - l_{c,K}(\boldsymbol{U}^{n,k-1}) - \mathscr{L}_{c,K}^{n,k,i+\nu} \right\|_K, \tag{67}$$

$$\eta_{\mathrm{rem},K,c}^{n,k,i,\nu} := h_K |K|^{-1} \varepsilon^{-\frac{1}{2}} \left\| \boldsymbol{R}_{c,K}^{n,k,i+\nu} \right\|_K. \tag{68}$$

The estimators defined previously reflect various violations of physical properties of the approximate numerical solution $\boldsymbol{U}^{n,k,i}$: the residual estimator $\eta_{\mathrm{R},K,c}^{n,k,i,\nu}$ illustrates the fact that the discrete flux reconstruction $\boldsymbol{\Theta}_{c,h}^{n,k,i,\nu}$ does not necessarily satisfy exactly the first two lines of (14). Note that, when the source term $Q_{c,K}^n$ is constant in time and space ($Q_{c,K}^n = Q_c$), (60) leads to $\eta_{\mathrm{R},K,c}^{n,k,i,\nu} = 0$. The flux estimator $\eta_{\mathrm{F},K,c}^{n,k,i,\nu}$ given by (64) indicates how far is the flux at the discrete level from the equilibrated flux reconstruction. It is related to the temporal discretization, linearization, and algebraic errors. Next, the nonconformity estimators (65)–(66) show how far are the discrete discontinuous quadratic liquid pressure and molar fraction of liquid hydrogen from their interpolants in the energy space X. Finally, the estimator (67) is the nonlinear accumulation estimator and (68) is the algebraic remainder estimator. Observe that at convergence of the semismooth solver and the iterative algebraic solver ($k \to \infty$, $i \to \infty$), the estimators (67) and (68) vanish.

The following result provides an upper bound for the error measure (53) at each semismooth Newton step $k \geq 1$ and each algebraic solver step $i \geq 0$ of each time step $1 \leq n \leq N_t$.

Theorem 3 *Consider a time step $1 \leq n \leq N_t$, a semismooth Newton step $k \geq 1$, an algebraic solver steps $i \geq 0$, and $\nu > 0$ additional algebraic iterations. Let $\left(S_h^{n,k,i}, P_h^{n,k,i}, \chi_h^{n,k,i}\right)$ be the approximate solution and let $\boldsymbol{\Theta}_{c,h}^{n,k,i,\nu}$, $\tilde{P}_{h\tau}^{n,k,i}$, and $\tilde{\chi}_{h\tau}^{n,k,i}$ be respectively the equilibrated flux reconstructions defined by (59), the liquid phase pressure reconstruction, and the molar fraction reconstruction defined in Section 5.5 with the convention (42). We have the following a posteriori error estimate*

$$\mathscr{N}^{n,k,i} \leq \left\{ \sum_{c\in\mathscr{C}} \left\{ \left\{ \int_{I_n} \sum_{K\in\mathscr{T}_h} \left(\eta_{\mathrm{R},K,c}^{n,k,i,\nu} + \eta_{\mathrm{F},K,c}^{n,k,i,\nu}(t) + \eta_{\mathrm{NA},K,c}^{n,k,i,\nu} + \eta_{\mathrm{rem},K,c}^{n,k,i,\nu} \right)^2 \mathrm{d}t \right\}^{\frac{1}{2}} + \left\| Q_c - Q_{c,h\tau} \right\|_{X_n'} \right\}^2 \right\}^{\frac{1}{2}} + \mathscr{R}_{\mathrm{e}}(S_{h\tau}^{n,k,i}, P_{h\tau}^{n,k,i}, \chi_{h\tau}^{n,k,i}) + \left\{ \int_{I_n} \sum_{K\in\mathscr{T}_h} \left\{ \sum_{c\in\mathscr{C}^l} \left(\eta_{\mathrm{NC},K,1,c}^{n,k,i}(t) \right)^2 + \left(\eta_{\mathrm{NC},K,\chi}^{n,k,i}(t) \right)^2 \right\} \mathrm{d}t \right\}^{\frac{1}{2}}. \tag{69}$$

Proof The proof follows the one presented in [29, Corollary 4.4] with the difference in the treatment of the algebraic remainder and the presence of the residual associated to the constraints. Let $\varphi \in X_n$ such that $\|\varphi\|_{X_n} = 1$. The residual (51) is given by

$$\langle \mathscr{R}_c(S_{h\tau}^{n,k,i}, P_{h\tau}^{n,k,i}, \chi_{h\tau}^{n,k,i}), \varphi \rangle_{X_n', X_n} = \int_{I_n} \sum_{K\in\mathscr{T}_h} A_K(\varphi)(t)\, \mathrm{d}t,$$

where

$$A_K(\varphi) := \left(Q_c - \partial_t l_{c,h\tau}^{n,k,i}, \varphi \right)_K + \left(\boldsymbol{\Phi}_{c,h\tau}^{n,k,i}, \nabla\varphi \right)_K.$$

Using (60) and noting that $\boldsymbol{\Theta}_{c,h}^{n,k,i,\nu} \in \mathbf{H}(\mathrm{div}, \Omega)$, we have

$$\begin{aligned} A_K(\varphi) = & \left(Q_{c,K}^n - \frac{l_{c,K}(\boldsymbol{U}^{n,k-1}) - l_{c,K}^{n-1} + \mathscr{L}_{c,K}^{n,k,i+\nu}}{\tau_n} - \nabla\cdot\boldsymbol{\Theta}_{c,h}^{n,k,i,\nu} - \frac{\boldsymbol{R}_{c,K}^{n,k,i+\nu}}{|K|}, \varphi \right)_K - \left(\boldsymbol{\Theta}_{c,h}^{n,k,i,\nu} - \boldsymbol{\Phi}_{c,h\tau}^{n,k,i}, \nabla\varphi \right)_K \\ & - \left(\partial_t^n l_{c,h\tau}^{n,k,i} - \frac{l_{c,K}(\boldsymbol{U}^{n,k-1}) - l_{c,K}^{n-1} + \mathscr{L}_{c,K}^{n,k,i+\nu}}{\tau_n}, \varphi \right)_K \\ & - \left(\frac{1}{|K|} \boldsymbol{R}_{c,K}^{n,k,i+\nu}, \varphi \right)_K + \left(Q_c - Q_{c,h\tau}, \varphi \right)_K. \end{aligned} \tag{70}$$

We bound separately each of the five terms in (70) denoted by $A_{j,K}(\varphi)$, $j = 1, \ldots, 5$. Observe from the equilibration property (60) that the first term $A_{1,K}(\varphi)$ in (70) is equal to

$$A_{1,K}(\varphi) := \left(Q_{c,K}^{n} - \frac{l_{c,K}(\boldsymbol{U}^{n,k-1}) - l_{c,K}^{n-1} + \mathscr{L}_{c,K}^{n,k,i+\nu}}{\tau_n} - \frac{\boldsymbol{R}_{c,K}^{n,k,i+\nu}}{|K|} - \nabla \cdot \boldsymbol{\Theta}_{c,h}^{n,k,i,\nu}, \varphi - \overline{\varphi}_K \right)_K, \quad (71)$$

where $\overline{\varphi}_K$ is the mean value of φ on $K \in \mathscr{T}_h$. Next, we have as a result of the Poincaré–Wirtinger inequality

$$\begin{aligned} \left\| \varphi - \overline{\varphi}_K \right\|_K (t) &\le h_K C_{\mathrm{PW}} \left\| \nabla \varphi \right\|_K (t), \\ &\le h_K C_{\mathrm{PW}} \left\| \varphi \right\|_{X,K} (t). \end{aligned}$$

Furthermore, observe that

$$\begin{aligned} \left\| \varphi - \overline{\varphi}_K \right\|_K (t) \le \left\| \varphi \right\|_K (t) &= \frac{\varepsilon^{\frac{1}{2}} \left\| \varphi \right\|_K (t) h_K^{-1}}{\varepsilon^{\frac{1}{2}} h_K^{-1}}, \\ &\le \frac{\left\| \varphi \right\|_{X,K} (t)}{\varepsilon^{\frac{1}{2}} h_K^{-1}}. \end{aligned} \quad (72)$$

Combining (71)–(72) provides the following upper bound:

$$A_{1,K}(\varphi) \le \eta_{\mathrm{R},K,c}^{n,k,i,\nu} \left\| \varphi \right\|_{X,K} (t). \quad (73)$$

Using the Cauchy–Schwarz inequality, the second term $A_{2,K}(\varphi)$ of (70) is obviously bounded as

$$A_{2,K}(\varphi) \le \eta_{\mathrm{F},K,c}^{n,k,i,\nu}(t) \left\| \varphi \right\|_{X,K} (t). \quad (74)$$

Concerning the third term $A_{3,K}(\varphi)$ of (70), observe first of all, employing (19), that it is equal to

$$A_{3,K}(\varphi) := \left(\frac{l_{c,K}(\boldsymbol{U}^{n,k,i}) - l_{c,K}(\boldsymbol{U}^{n,k-1}) - \mathscr{L}_{c,K}^{n,k,i+\nu}}{\tau_n}, \varphi \right)_K. \quad (75)$$

To bound (75), we use the Cauchy–Schwarz inequality giving

$$A_{3,K}(\varphi) \le \eta_{\mathrm{NA},K,c}^{n,k,i,\nu} \varepsilon^{\frac{1}{2}} h_K^{-1} \left\| \varphi \right\|_K \le \eta_{\mathrm{NA},K,c}^{n,k,i,\nu} \left\| \varphi \right\|_{X,K}. \quad (76)$$

To bound the space integral $A_{4,K}(\varphi)$ containing the algebraic remainder, we employ the Cauchy–Schwarz inequality and next the definition of the error measure (43) to get

$$\begin{aligned} A_{4,K}(\varphi) &\le \frac{1}{|K|} \left\| \boldsymbol{R}_{c,K}^{n,k,i+\nu} \right\|_K \varepsilon^{-\frac{1}{2}} h_K \left\| \varphi \right\|_{X,K} (t), \\ &= \eta_{\mathrm{rem},K,c}^{n,k,i,\nu} \left\| \varphi \right\|_{X,K} (t). \end{aligned} \quad (77)$$

Finally, concerning the last bound $A_{5,K}(\varphi)$ we use

$$\int_{I_n} \left(Q_c - Q_{c,h\tau}, \varphi \right)_\Omega (t) \, \mathrm{d}t \le \left\| Q_c - Q_{c,h\tau} \right\|_{X_n'} \left\| \varphi \right\|_{X_n}. \quad (78)$$

Thus, as $\left\| \varphi \right\|_{X_n} = 1$, combining (70), (73), (74), (76), (77), and (78) and using the Cauchy–Schwarz inequality, we get

$$\begin{aligned} &\left\| \mathscr{R}_c(S_{h\tau}^{n,k,i}, P_{h\tau}^{n,k,i}, \chi_{h\tau}^{n,k,i}) \right\|_{X_n'} \\ &\le \left\{ \int_{I_n} \sum_{K \in \mathscr{T}_h} \left(\eta_{\mathrm{R},K,c}^{n,k,i,\nu} + \eta_{\mathrm{F},K,c}^{n,k,i,\nu}(t) + \eta_{\mathrm{NA},K,c}^{n,k,i,\nu} \right. \right. \\ &\quad \left. \left. + \eta_{\mathrm{rem},K,c}^{n,k,i,\nu} \right)^2 \mathrm{d}t \right\}^{\frac{1}{2}} + \left\| Q_c - Q_{c,h\tau} \right\|_{X_n'}. \end{aligned} \quad (79)$$

Next, as $\tilde{P}_{h\tau}^{n,k,i} \in X_n$ and $\tilde{\chi}_{h\tau}^{n,k,i} \in X_n$, we deduce from (54) and (55) that

$$\mathscr{N}_P^{n,k,i}(P_{h\tau}^{n,k,i}) \le \left\{ \sum_{c \in \mathscr{C}} \int_{I_n} \sum_{K \in \mathscr{T}_h} \left(\eta_{\mathrm{NC},K,1,c}^{n,k,i}(t) \right)^2 \mathrm{d}t \right\}^{\frac{1}{2}} \quad (80)$$

and

$$\mathscr{N}_\chi^{n,k,i}(\chi_{h\tau}^{n,k,i}) \le \left\{ \int_{I_n} \sum_{K \in \mathscr{T}_h} \left(\eta_{\mathrm{NC},K,\chi}^{n,k,i}(t) \right)^2 \mathrm{d}t \right\}^{\frac{1}{2}}. \quad (81)$$

Thus, combining (79)–(81) we get the desired result. □

So far, we have established an a posteriori estimate between the exact and the approximate solution. We now provide an estimate distinguishing the different error components. For this purpose, we additionally define the positive and negative parts of each constraint as follows. For A, any real number, we define

$$\begin{aligned} &A = A^+ + A^-, \quad \text{with} \quad A^+ := \max(0, A) \ge 0, \\ &\text{and} \quad A^- := \min(0, A) \le 0. \end{aligned} \quad (82)$$

Definition 3 Let $1 \le n \le N_t$ be a time step, $k \ge 1$ be a semismooth Newton iteration, and $i \ge 0$ be an algebraic iteration. For any $c \in \mathscr{C}$, we define the discretization estimator, the linearization estimator, and the algebraic estimator by

$$\begin{aligned} &\eta_{\mathrm{disc}}^{n,k,i,\nu} \\ &:= 2^{\frac{1}{2}} \left\{ \sum_{K \in \mathscr{T}_h} \int_{I_n} \left\{ \sum_{c \in \mathscr{C}} \left(\eta_{\mathrm{R},K,c}^{n,k,i,\nu} \right. \right. \right. \\ &\quad \left. + \left\| \boldsymbol{\Theta}_{c,h,\mathrm{disc}}^{n,k,i} - \boldsymbol{\Phi}_{c,h\tau}^{n,k,i}(t) \right\|_K + \eta_{\mathrm{NC},K,1,c}^{n,k,i}(t) \right) \\ &\quad \left. \left. + \eta_{\mathrm{NC},K,\chi}^{n,k,i}(t) \right\}^2 \mathrm{d}t \right\}^{\frac{1}{2}} + \frac{1}{\alpha} \sum_{K \in \mathscr{T}_h} \int_{I_n} \eta_{\mathrm{P},K,\mathrm{pos}}^{n,k,i}(t) \, \mathrm{d}t \end{aligned} \quad (83)$$

$$\begin{aligned} \eta_{\mathrm{lin}}^{n,k,i} &:= \left\{ \sum_{c \in \mathscr{C}} \tau_n \sum_{K \in \mathscr{T}_h} \left(\left\| \boldsymbol{\Theta}_{c,h,\mathrm{lin}}^{n,k,i} \right\|_K + \eta_{\mathrm{NA},K,c}^{n,k,i,\nu} \right)^2 \right\}^{\frac{1}{2}} \\ &\quad + \frac{1}{\alpha} \sum_{K \in \mathscr{T}_h} \int_{I_n} \eta_{\mathrm{P},K,\mathrm{neg}}^{n,k,i}(t) \, \mathrm{d}t, \end{aligned} \quad (84)$$

$$\eta_{\mathrm{alg}}^{n,k,i,\nu} := \left\{ \sum_{c\in\mathscr{C}} \tau_n \sum_{K\in\mathscr{T}_h} \left(\left\| \boldsymbol{\Theta}_{c,h,\mathrm{alg}}^{n,k,i,\nu} \right\|_K + \eta_{\mathrm{rem},K,c}^{n,k,i,\nu} \right)^2 \right\}^{\frac{1}{2}}, \tag{85}$$

with

$$\eta_{\mathrm{P},K,\mathrm{pos}}^{n,k,i}(t) := \left(\left\{ 1 - S_{h\tau}^{n,k,i}(t) \right\}^+, \left\{ H\left[P_{h\tau}^{n,k,i}(t) + P_{\mathrm{cp}}\left(S_{h\tau}^{n,k,i}(t) \right) \right] - \beta^{\mathrm{l}} \chi_{h\tau}^{n,k,i}(t) \right\}^+ \right)_K, \tag{86}$$

$$\eta_{\mathrm{P},K,\mathrm{neg}}^{n,k,i}(t) := \left(\left\{ 1 - S_{h\tau}^{n,k,i}(t) \right\}^-, \left\{ H\left[P_{h\tau}^{n,k,i}(t) + P_{\mathrm{cp}}\left(S_{h\tau}^{n,k,i}(t) \right) \right] - \beta^{\mathrm{l}} \chi_{h\tau}^{n,k,i}(t) \right\}^- \right)_K. \tag{87}$$

Remark 4 In Definition 3, we proposed three components of the error constructed from the various estimators defined in Section 5.6. Note that it is possible to bound the residual $\mathscr{R}_{\mathrm{e}}$ following the decomposition (82) and employing the property

$$A_1 A_2 = \left[A_1^+ + A_1^- \right] \left[A_2^+ + A_2^- \right] \le A_1^+ A_2^+ + A_1^- A_2^-. \tag{88}$$

The phase transition estimators $\eta_{\mathrm{P},K,\mathrm{pos}}^{n,k,i}(t)$ and $\eta_{\mathrm{P},K,\mathrm{neg}}^{n,k,i}(t)$ given by (86) and (87) are new to the best of our knowledge and give a control on the violation of the constraints: they evaluate the error due to the physical phase change between the liquid and the liquid–gas phase. At convergence of the semismooth and linear algebraic solver ($k \to \infty$, $i \to \infty$) $\eta_{\mathrm{P},K,\mathrm{neg}}^{n,\infty,\infty}(t) = 0$. Observe that when the gas phase appears in the triangle K, the estimator $\eta_{\mathrm{P},K,\mathrm{pos}}^{n,\infty,\infty}(t)$ is positive on the time interval corresponding to the state change. Otherwise it is vanishing. Therefore, our approach is heuristic in the sense that at convergence of the iterative algebraic solver and the semismooth solver $\eta_{\mathrm{lin}}^{n,k,i} \to 0$ and $\eta_{\mathrm{alg}}^{n,k,i,\nu} \to 0$. Note that the algebraic remainder estimator is always positive then when added to $\left\| \boldsymbol{\Theta}_{c,h,\mathrm{alg}}^{n,k,i,\nu} \right\|_K$ provides a non vanishing global algebraic estimator at the beginning of the iterations.

Corollary 1 *For a given time step $1 \le n \le N_t$, a semismooth Newton iteration $k \ge 1$, an algebraic iteration $i \ge 0$, and $\nu > 0$ additional algebraic sover steps, consider the estimators defined by (83)–(85). Assume moreover that the source term Q_c is piecewise constant in space and time. Then, we have*

$$\mathscr{N}^{n,k,i} \le \eta_{\mathrm{disc}}^{n,k,i,\nu} + \eta_{\mathrm{lin}}^{n,k,i} + \eta_{\mathrm{alg}}^{n,k,i,\nu}.$$

Proof The triangle inequality applied on the flux estimator gives

$$\eta_{\mathrm{F},K,c}^{n,k,i,\nu}(t) \le \left\| \boldsymbol{\Theta}_{c,h,\mathrm{disc}}^{n,k,i} - \boldsymbol{\Phi}_{c,h\tau}^{n,k,i}(t) \right\|_K + \left\| \boldsymbol{\Theta}_{c,h,\mathrm{lin}}^{n,k,i} \right\|_K + \left\| \boldsymbol{\Theta}_{c,h,\mathrm{alg}}^{n,k,i,\nu} \right\|_K. \tag{89}$$

Plugging (89) in (69), and using after the Minkowski inequality to separate each component fluxes and each nonconform estimators provides the following bound for (69)

$$\begin{aligned} \mathscr{N}^{n,k,i} \le & \left\{ \sum_{c\in\mathscr{C}} \int_{I_n} \sum_{K\in\mathscr{T}_h} \left(\eta_{\mathrm{R},K,c}^{n,k,i,\nu} + \left\| \boldsymbol{\Theta}_{c,h,\mathrm{disc}}^{n,k,i} - \boldsymbol{\Phi}_{c,h\tau}^{n,k,i}(t) \right\|_K \right)^2 \mathrm{dt} \right\}^{\frac{1}{2}} \\ & + \mathscr{R}_{\mathrm{e}}(S_{h\tau}^{n,k,i}, P_{h\tau}^{n,k,i}, \chi_{h\tau}^{n,k,i}) \\ & + \left\{ \int_{I_n} \sum_{K\in\mathscr{T}_h} \left\{ \sum_{c\in\mathscr{C}^{\mathrm{l}}} \left(\eta_{\mathrm{NC},K,\mathrm{l},c}^{n,k,i}(t) \right)^2 + \left(\eta_{\mathrm{NC},K,\chi}^{n,k,i}(t) \right)^2 \right\} \mathrm{dt} \right\}^{\frac{1}{2}} \\ & + \left\{ \sum_{c\in\mathscr{C}} \tau_n \sum_{K\in\mathscr{T}_h} \left(\left\| \boldsymbol{\Theta}_{c,h,\mathrm{lin}}^{n,k,i} \right\|_K + \eta_{\mathrm{NA},K,c}^{n,k,i,\nu} \right)^2 \right\}^{\frac{1}{2}} \\ & + \eta_{\mathrm{alg}}^{n,k,i,\nu}. \end{aligned} \tag{90}$$

To bound $\mathscr{R}_{\mathrm{e}}(S_{h\tau}^{n,k,i}, P_{h\tau}^{n,k,i}, \chi_{h\tau}^{n,k,i})$ we employ (88) to get $\mathscr{R}_{\mathrm{e}}(S_{h\tau}^{n,k,i}, P_{h\tau}^{n,k,i}, \chi_{h\tau}^{n,k,i}) \le \frac{1}{\alpha} \int_{I_n} \sum_{K\in\mathscr{T}_h} \left(\eta_{\mathrm{P},K,\mathrm{pos}}^{n,k,i} + \eta_{\mathrm{P},K,\mathrm{neg}}^{n,k,i} \right) \mathrm{dt}$. To conclude, it remains to bound the sum of the first and third term of (90). To do so, we employ the inequality $\left(\sum_{q=1}^r X_q^2 \right)^{\frac{1}{2}} + \left(\sum_{q=1}^r Y_q^2 \right)^{\frac{1}{2}} \le \left(2 \sum_{q=1}^r \left(X_q^2 + Y_q^2 \right) \right)^{\frac{1}{2}}$ for all $X_q, Y_q \ge 0$ and next the identity $A^2 + B^2 \le (A+B)^2$ for all $A, B \ge 0$ to obtain the desired result. □

5.7 Adaptive inexact semismooth Newton method using adaptive stopping criteria

In this section, we develop an adaptive inexact semismooth Newton method. In the spirit of [5, 26, 32, 54], it is designed to perform the linearization and algebraic resolution with minimal necessary precision and thus to avoid unnecessary iterations. We rely on Corollary 1 that estimates the different error components.

We define γ_{lin} and γ_{alg} as two positive parameters representing the desired relative size of the algebraic and linearization errors. We propose the following stopping

criteria, balancing globally the algebraic, linearization, and discretization error components for our adaptive algorithm (see Algorithm 1)

$$\text{(a) } \eta_{\text{alg}}^{n,k,i,\nu} \leq \gamma_{\text{alg}} \max\left\{\eta_{\text{disc}}^{n,k,i,\nu}, \eta_{\text{lin}}^{n,k,i}\right\}, \quad \text{(b) } \eta_{\text{lin}}^{n,k,i} \leq \gamma_{\text{lin}} \eta_{\text{disc}}^{n,k,i,\nu}. \tag{91}$$

We propose the following adaptive inexact semismooth algorithm:

Algorithm 1 Adaptive inexact semismooth Newton algorithm.

0. Choose an initial vector $\boldsymbol{U}^{n,0} \in \mathbb{R}^{3N_{\text{sp}}}$ and set $k = 1$.

1. From $\boldsymbol{U}^{n,k-1}$ define $\mathbb{A}^{n,k-1} \in \mathbb{R}^{3N_{\text{sp}},3N_{\text{sp}}}$ and $\boldsymbol{B}^{n,k-1} \in \mathbb{R}^{3N_{\text{sp}}}$ by (36) and (37).

2. Consider the linear system

$$\mathbb{A}^{n,k-1}\boldsymbol{U}^{n,k} = \boldsymbol{B}^{n,k-1}. \tag{92}$$

3. Set $\boldsymbol{U}^{n,k,0} = \boldsymbol{U}^{n,k-1}$ as initial guess for the iterative linear solver, set $i = 0$.

4*a*. Perform $\nu \geq 1$ steps of a chosen linear solver for (92), starting from $\boldsymbol{U}^{n,k,i}$.

This yields on step $i + \nu$ an approximation $\boldsymbol{U}^{n,k,i+\nu}$ to $\boldsymbol{U}^{n,k}$ satisfying

$$\mathbb{A}^{n,k-1}\boldsymbol{U}^{n,k,i+\nu} = \boldsymbol{B}^{n,k-1} - \boldsymbol{R}^{n,k,i+\nu}.$$

4*b*. Compute the estimators of Definition 3 and check the stopping criterion for the linear solver in the form (91)(a). Set $i = i+\nu$. If satisfied, set $\boldsymbol{U}^{n,k} = \boldsymbol{U}^{n,k,i}$. If not go back to 4*a*.

5. Check the stopping criterion for the nonlinear solver in the form (91)(b). If satisfied, return $\boldsymbol{U}^{n} = \boldsymbol{U}^{n,k}$. If not, set $k = k + 1$ and go back to 1.

6 Numerical experiments

6.1 Setting

This section illustrates numerically our theoretical developments. We use the Couplex-gas benchmark proposed by Andra (French National Inventory of Radioactive Materials and Waste)[1] and the research group MoMaS (Mathematical Modeling and Numerical Simulation for Nuclear Waste Management Problems)[2].

[1] http://www.andra.fr/international/

[2] http://www.gdrmomas.org/ex_qualifications.html/

We consider a homogeneous porous medium Ω in one dimension supposed to be horizontal with length $L = 200$ m. Its constant porosity is fixed to $\phi = 0.15$ and its constant absolute permeability is equal to $\underline{\mathbf{K}} = 5 \times 10^{-20}$ m^2. The porous medium is initially saturated with liquid ($S^{\text{l}} = 1$) and contains no hydrogen ($\chi_{\text{h}}^{\text{l}} = 0$). We assume that gaseous hydrogen is injected constantly in time in the first cell K_1 ($Q_{\text{h},K_1}^{n} = 5.57 \times 10^{-6}$ kg/m^2/year) and the water flow rate is zero. We have homogeneous Neumann boundary conditions on the left of the domain. For boundary conditions on the right, we assume that the gas injected will never reach the end of the domain, thus Dirichlet conditions are prescribed ($S^{\text{l}} = 1$, $P^{\text{l}} = 10^6$Pa, $\chi_{\text{h}}^{\text{l}} = 0$). As we consider a horizontal 1D case, gravitational effects are not taken into account in the numerical tests. The dynamic liquid phase viscosity $\mu^{\text{l}} = 10^{-9}$ Pa$\cdot$s, the dynamic gas phase viscosity $\mu^{\text{g}} = 9 \times 10^{-9}$ Pa$\cdot$s, the molar mass of water $M_{\text{w}} = 10^{-2}$ kg$\cdot$mol^{-1}, the molar mass of hydrogen $M_{\text{h}} = 2 \times 10^{-3}$ kg$\cdot$mol^{-1}, the molar density of water $\rho_{\text{w}}^{\text{l}} = 10^3$ kg$\cdot$m^{-3}, the molecular diffusion coefficient $D_{\text{h}}^{\text{l}} = 3 \times 10^{-9}$ m$\cdot$s^{-1}, and Henry's constant $\tilde{H} = 7.65 \times 10^{-6}$ mol Pa$^{-1}\cdot$m^{-3}. We consider for the capillary pressure P_{cp} and the relative permeability of the liquid phase k_{r}^{l} and gas phase k_{r}^{g} the Van Genuchten–Mualem model:

$$P_{\text{cp}}(S^{\text{l}}) = P_{\text{r}}\left(S_{\text{le}}^{-\frac{1}{m}} - 1\right)^{\frac{1}{n^*}},$$
$$k_{\text{r}}^{\text{l}}(S^{\text{l}}) = \sqrt{S_{\text{le}}}\left(1 - \left(1 - S_{\text{le}}^{\frac{1}{m}}\right)^{m}\right)^{2},$$
$$k_{\text{r}}^{\text{g}}(S^{\text{l}}) = \sqrt{1 - S_{\text{le}}}\left(1 - S_{\text{le}}^{\frac{1}{m}}\right)^{2m},$$

with

$$S_{\text{le}} = \frac{S^{\text{l}} - S_{\text{res}}^{\text{l}}}{1 - S_{\text{res}}^{\text{l}} - S_{\text{res}}^{\text{g}}} \quad \text{and} \quad m = 1 - \frac{1}{n^*}.$$

Here $P_{\text{r}} = 2 \times 10^6$Pa is the reference pressure, $n^* = 1.49$ is a parameter depending on the porous medium, and $S_{\text{res}}^{\text{l}} = 0.4$, $S_{\text{res}}^{\text{g}} = 0$ are respectively the residual liquid saturation and residual gas saturation (see for more details [18]). We consider a uniform spatial mesh ($N_{\text{sp}} = 1000$ elements) and we use a constant time step $\tau_n = 5000$ years $\forall 1 \leq n \leq N_t$. The final time of simulation is $t_{\text{F}} = 5 \times 10^5$ years and the rescaling constant $\alpha = 2500$ years.

We consider two different semismooth Newton solvers. We first employ the Newton-min algorithm combined with the GMRES linear iterative algebraic solver for the system (35). Next, we employ the Newton–Fischer–Burmeister algorithm in combination with the GMRES solver. In both cases, an ILU preconditionner is used to speed up the GMRES solver. Other possibilities for preconditionners can be found in [50] and the references therein. For the

computation of the algebraic flux reconstruction $\boldsymbol{\Theta}_{c,h,\mathrm{alg}}^{n,k,i,\nu}$, we use (58) with $\nu = 1$. We also define the algebraic and linearization residuals by

$$\boldsymbol{R}_{\mathrm{alg}}^{n,k,i} := \boldsymbol{B}^{n,k-1} - \mathbb{A}^{n,k-1}\boldsymbol{U}^{n,k,i}, \tag{93}$$

$$\boldsymbol{R}_{\mathrm{lin}}^{n,k,i} := \begin{bmatrix} \mathscr{H}^n(\boldsymbol{U}^{n,k,i}) \\ \mathscr{C}^n(\boldsymbol{U}^{n,k,i}) \end{bmatrix}, \tag{94}$$

where the nonlinear operators $\mathscr{H}^n$ and $\mathscr{C}^n$ are defined in (30) and (33).

Three different approaches are tested:

1. The *exact* semismooth Newton method. Here, both the linear and nonlinear solvers are iterated to "almost" convergence. More precisely, we take $\varepsilon_{\mathrm{alg}} = 10^{-12}$ and $\varepsilon_{\mathrm{lin}} = 10^{-7}$ and replace respectively the stopping criteria (91) of Algorithm 1 by criteria on the relative residuals,

$$\text{(a)}\ \frac{\left\|\boldsymbol{R}_{\mathrm{alg}}^{n,k,i}\right\|}{\left\|\boldsymbol{B}^{n,k-1}\right\|} \le \varepsilon_{\mathrm{alg}}, \qquad \text{(b)}\ \frac{\left\|\boldsymbol{R}_{\mathrm{lin}}^{n,k,i}\right\|}{\left\|\mathscr{F}(\boldsymbol{U}^{n,0})\right\|} \le \varepsilon_{\mathrm{lin}}. \tag{95}$$

2. The *inexact* semismooth Newton method. Here, (35) is solved only approximately. We use the following stopping criterion replacing (95)(a) for the iterative algebraic solver:

$$\text{(a)}\ \frac{\left\|\boldsymbol{R}_{\mathrm{alg}}^{n,k,i}\right\|}{\left\|\boldsymbol{B}^{n,k-1}\right\|} \le \Gamma_k. \tag{96}$$

   In the literature, Γ_k is called the "forcing term" and under the assumption that the sequence $(\Gamma_k)_{k\ge1}$ is uniformly less than 1, inexact Newton methods are locally convergent (see [27, 47]). We choose

$$\Gamma_k = \frac{1}{2^k}\frac{\left\|\boldsymbol{R}_{\mathrm{lin}}^{n,k,i}\right\|}{\left\|\mathscr{F}(\boldsymbol{U}^{n,0})\right\|}. \tag{97}$$

   Concerning the stopping criterion for the semismooth Newton solver, we keep (95) (b).

3) The *adaptive inexact* semismooth Newton method (see Algorithm 1) that relies on the stopping criteria (91)(a) and (91)(b) with $\gamma_{\mathrm{alg}} = 10^{-3}$ and $\gamma_{\mathrm{lin}} = 10^{-3}$.

For the three methods, the criteria are computed every $\nu = 1$ linear iteration. In the sequel, when the stopping criterion of the nonlinear solver is satisfied, the index k will be denoted by $\bar{k}$, and similarly the index i at the various stopping criteria will be denoted by $\bar{i}$.

6.2 Newton-min

We consider the $2 \times N_{\mathrm{sp}}$ equations given by the cell-centered finite volume discretization (28), where we recall that N_{sp} equations correspond to each component $c \in \mathscr{C}$. The nonlinear complementarity constraints are reformulated thanks to the semismooth min function as follows: $\forall K \in \mathscr{T}_h$, $\forall 1 \le n \le N_t$

$$\begin{aligned} &1 - S_K^n \ge 0, \quad H\left[P_K^n + P_{\mathrm{cp}}(S_K^n)\right] - \beta^1 \chi_K^n \ge 0, \\ &\left[1 - S_K^n\right]\left[H\left[P_K^n + P_{\mathrm{cp}}(S_K^n)\right] - \beta^1 \chi_K^n\right] = 0, \\ &\iff \min\left(1 - S_K^n, H\left[P_K^n + P_{\mathrm{cp}}(S_K^n)\right] - \beta^1 \chi_K^n\right) = 0. \end{aligned}$$

We then employ the Newton-min solver to treat the nonlinearities.

Figure 1 displays the behavior of the solution at time $t = 1.05 \times 10^5$ years (corresponding to a two-phase regime) when the Newton-min and the GMRES solvers have converged. We observe from the three figures that the liquid pressure and the molar fraction of liquid hydrogen have increased almost everywhere and that the gas has spread in several cells of the domain. It is characteristic of a two-phase flow after appearance of the gas phase.

Figure 2 shows the possible violations of the nonlinear complementarity constraints during the iterations at the time step $t = 5 \times 10^4$ years (see the beginning of Section 5.6). We have represented in the left figure the negative part of the saturation constraint $\left\{1 - S_{h\tau}^{n,k,i}\right\}^-$ and we observe its negativity in several cells. The same phenomenon occurs for the constraint given by Henry's law (see the right figure).

In Fig. 3, we have displayed the behavior of the phase transition estimator $\eta_{\mathrm{P},K,\mathrm{pos}}^{n,k,i}(t)$ as a function of the abscissa at convergence ($k = \bar{k}$, $i = \bar{i}$). We recall that $\eta_{\mathrm{P},K,\mathrm{pos}}^{n,k,i}(t^n) = 0$ for all endpoints of all intervals I_n, $1 \le n \le N_t$ (see (86)–(87)) so the estimator is shown in the middle of the time interval I_n, denoted by $t_n^\star$. In the left figure, we have chosen I_1 ($t_1^\star = 2500$ years), during which there is only one liquid phase and one observes that $\eta_{\mathrm{P,K}}^{n,k,i}(t) = 0$ over all $t \in I_1$. On the middle figure, the estimator is shown at $t_3^\star = 1.25 \times 10^4$ years (corresponding time interval I_3). It corresponds to the time interval when the gas phase starts to appear in the leftmost cell, which can be observed on the estimator. Then, in several cells close to the left boundary, we observe a peak corresponding to the activation of the two constraints $1 - S_{h\tau}^{n,k,i}(\cdot, t_3^\star) > 0$ and $H\left[P_{h\tau}^{n,k,i}(\cdot, t_3^\star) + P_{\mathrm{cp}}(S_{h\tau}^{n,k,i}(\cdot, t_3^\star))\right] - \beta^1 \chi_{h\tau}^{n,k,i}(\cdot, t_3^\star) > 0$, then the nonnegativity of the estimator. In the right figure, the estimator $\eta_{\mathrm{P,K}}^{n,k,i}(t_9^\star)$ is shown at $t_9^\star = 4.25 \times 10^4$ years, when the flow is two-phase liquid–gas. We see the localization (near 45 m) of the gas phase appearance on the domain Ω by a peak. Thus, the front between the one-phase and the two-phase regimes can be clearly noted thanks to the estimator.

Remark 5 From this example, one can see that this estimator detects the error caused by the appearance of the gas phase whenever the gas spreads throughout the domain.

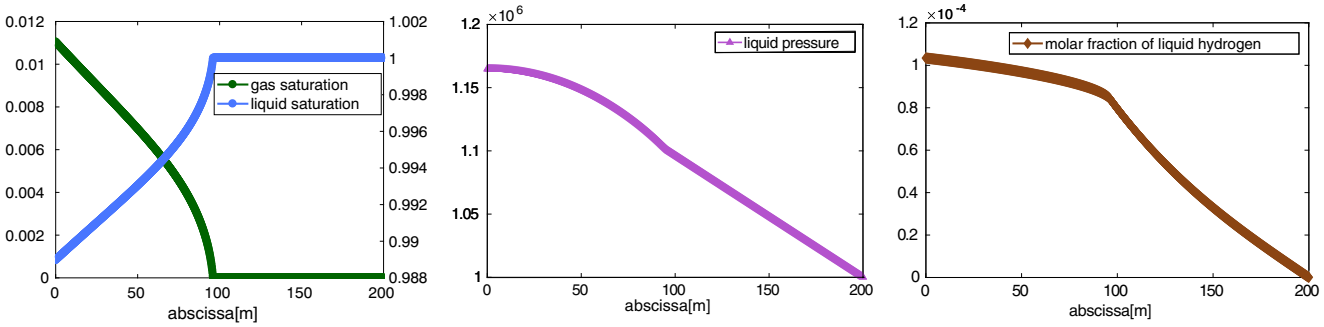

Fig. 1 Solution at convergence ($k = \overline{k}, i = \overline{i}$) for $N_{\text{sp}} = 1000$ elements at $t = 1.05 \times 10^5$ years. Left: saturation of the phases, middle: pressure of the liquid phase, right: molar fraction of liquid hydrogen

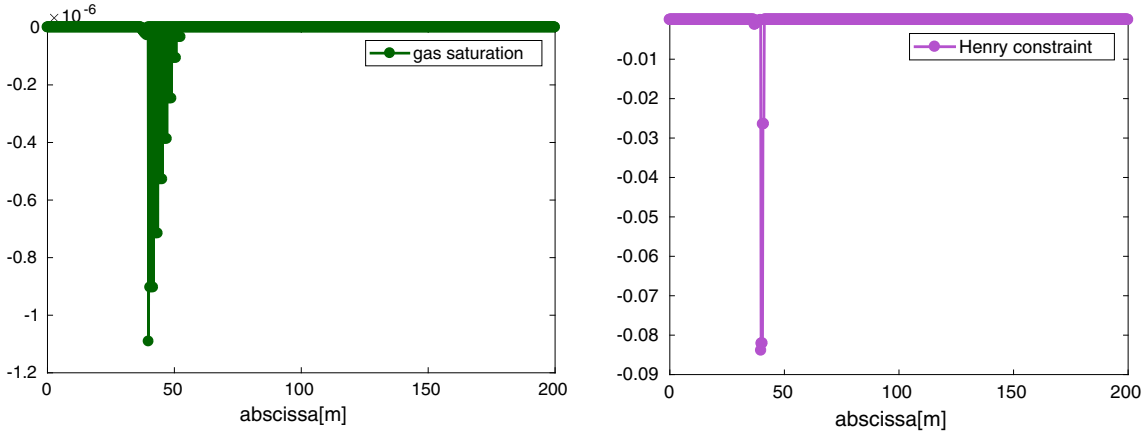

Fig. 2 Complementarity constraints ($k = 4, i = 2$) at time $t = 5 \times 10^4$ years. Left: negative part of the saturation constraint, right: negative part of Henry's constraint

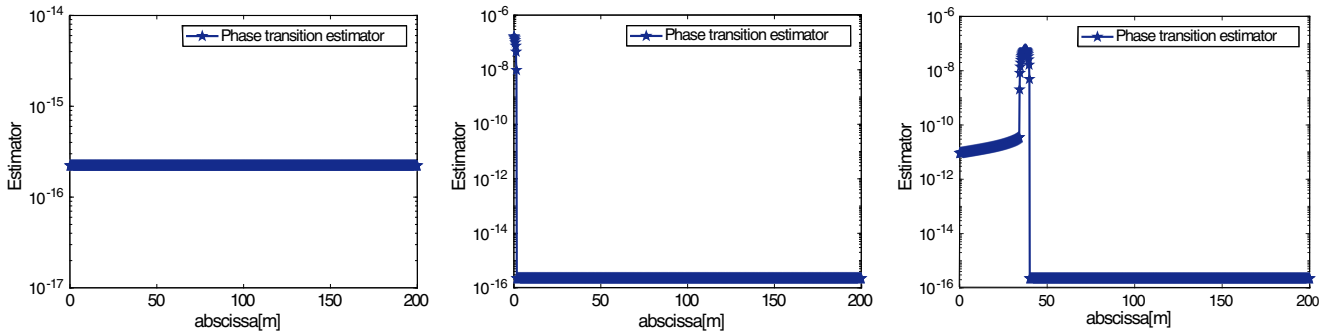

Fig. 3 Phase transition estimator $\eta^{n,k,i}_{\text{P},K,\text{pos}}$ at convergence ($k = \overline{k}, i = \overline{i}$). Left: one-phase liquid. middle: appearance of gas phase, right: two-phase liquid–gas

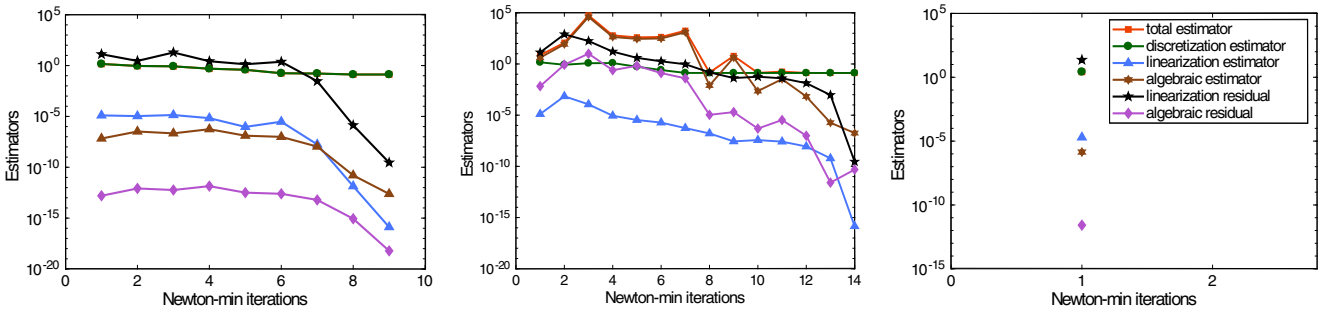

Fig. 4 Estimators as a function of the Newton-min iterates k, $(i = \bar{i})$ at $t = 1.05 \times 10^5$. Exact (left), inexact (middle), and adaptive inexact (right) Newton-min methods

It gives important tools for adaptive mesh refinement strategy that will be considered in a future work.

Figure 4 represents at the fixed time value $t = 1.05 \times 10^5$ years the evolution of the various estimators and the behavior of the nonrelative residuals $\left\| \boldsymbol{R}_{\text{lin}}^{n,k,i} \right\|$ and $\left\| \boldsymbol{R}_{\text{alg}}^{n,k,i} \right\|$ given by (93) and (94) as a function of the Newton-min iterations when the stopping criteria (95)(a)–(95)(b), (96)(a)–(95)(b), and (91)(a)–(91)(b) respectively have been satisfied (1000 elements, k varies, $i = \bar{i}$). In the exact resolution case, the discretization estimator globally dominates and coincides with the total estimator (the red and green curves are superimposed). The linearization estimator is small and decreases rapidly after $k = 6$. The algebraic estimator is small and takes values between 10^{-6} and 10^{-12}. Observe that the behavior of the linearization estimator (respectively algebraic estimator) mimics the one of the linearization residual (respectively algebraic residual) up to an important roughly constant shift. Note that the stopping criteria for exact and inexact Newton-min are based on the relative linearization and algebraic residuals (see (95)(a)–(95(b)) which do not correspond to the curves of $\left\| \boldsymbol{R}_{\text{lin}}^{n,k,i} \right\|$ and $\left\| \boldsymbol{R}_{\text{alg}}^{n,k,i} \right\|$ that are nonrelative residuals. From the first Newton-min iteration, the discretization estimator is more or less constant, which means that the other components of the error do not influence the behavior of the total error estimator. Therefore, the semismooth linearization iterations can be stopped at the first Newton-min step. This is precisely the situation described the by our adaptive inexact Newton-min (figure on the right). We have displayed in the figure in the middle the number of Newton-min iterations required to satisfy the inexact stopping criterion (95) (b). We observe that the inexact method requires more semismooth Newton-min iterations to converge (14 iterations) than the exact one.

Figure 5 shows the evolution of the various estimators and the behavior of $\left\| \boldsymbol{R}_{\text{lin}}^{n,k,i} \right\|$ and $\left\| \boldsymbol{R}_{\text{alg}}^{n,k,i} \right\|$ given by (93) and (94) during the algebraic iterations of the first Newton-min step (1000 elements, $k = 1$, i varies). In the three methods, the algebraic estimator is dominant and dominates the total estimator whereas the discretization and linearization estimators roughly stagnate. We observe that 3 GMRES iterations are needed to achieve the stopping criterion (95)(a) whereas in the inexact and adaptive inexact cases, 1 iteration and 3 iterations respectively are required to satisfy the stopping criteria (96)(a) and (91)(a). For the three methods, the estimators are computed every $\nu = 1$ iteration.

In Fig. 6, the number of Newton-min iterations and the total number of GMRES iterations required to satisfy the various stopping criteria at each time step of the simulation are displayed . In particular, the first graph shows

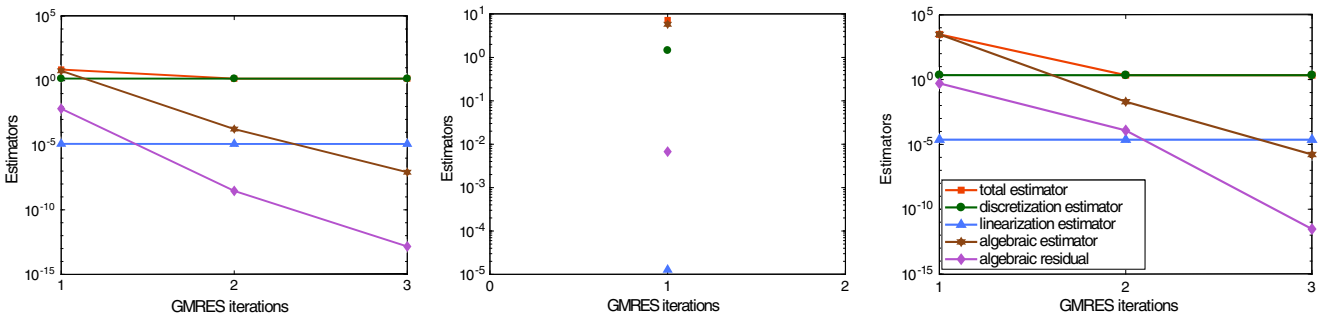

Fig. 5 Estimators as a function of the algebraic iterations i for $k = 1$ at $t = 1.05 \times 10^5$. Exact (left), inexact (middle), and adaptive inexact (right) semismooth Newton-min methods

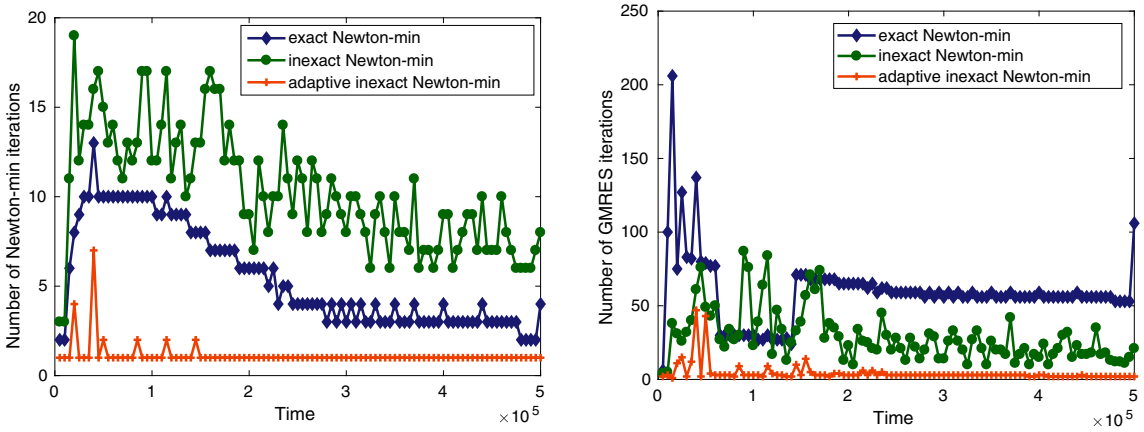

Fig. 6 Number of Newton-min iterations at each time step (left), number of GMRES iterations at each time step (right)

that the inexact Newton-min method requires many more semismooth iterations to converge in comparison with the other methods. The second graph of Fig. 6 shows that the exact Newton-min method is globally the most expensive method in terms of linear algebraic iterations and adaptive inexact Newton-min method is the cheapest one.

Figure 7 illustrates the overall performance of the three approaches. In the first graph, the cumulated number of Newton-min iterations for the three methods is displayed as a function of the time steps. The inexact Newton-min method requires approximately 1000 Newton-min iterations in total whereas exact Newton-min and adaptive inexact Newton-min require 550 iterations and 100 iterations respectively. The right part of Fig. 7 focuses on the cumulated number of GMRES iterations for each method as a function of the time step. The adaptive inexact Newton-min method is the least expensive since it requires approximately 500 iterations whereas inexact Newton-min and adaptive inexact Newton-min require 3000 iterations and 6000 iterations respectively, to finish the simulation. Thus, globally our approach yields an economy by a factor of roughly 6 with respect to inexact Newton-min and roughly 12 with respect to exact Newton-min in terms of total algebraic solver iterations.

In the three first graphs of Fig. 8, the behavior of the solution at convergence ($k = \bar{k}$, $i = \bar{i}$) at the selected time $t = 1.05 \times 10^5$ years for the exact Newton-min resolution and adaptive inexact Newton-min resolution with the weights $\gamma_{\text{alg}} = \gamma_{\text{lin}} = 10^{-3}$ is displayed. We observe a non-consistency zone for the three graphs explained by the nonlinear stopping criterion in adaptive inexact resolution that stops earlier the semismooth iterations. The next three graphs of Fig. 8 show that at a time close to the final simulation time ($t = 3.5 \times 10^5$ years), the curves of the solutions given by exact Newton-min and adaptive inexact Newton-min almost coincide. Thus, our adaptive inexact semimooth Newton algorithm saves many Newton-min and GMRES iterations and generates a solution whose precision does not differ from the exact one more than by a fraction of the discretization error.

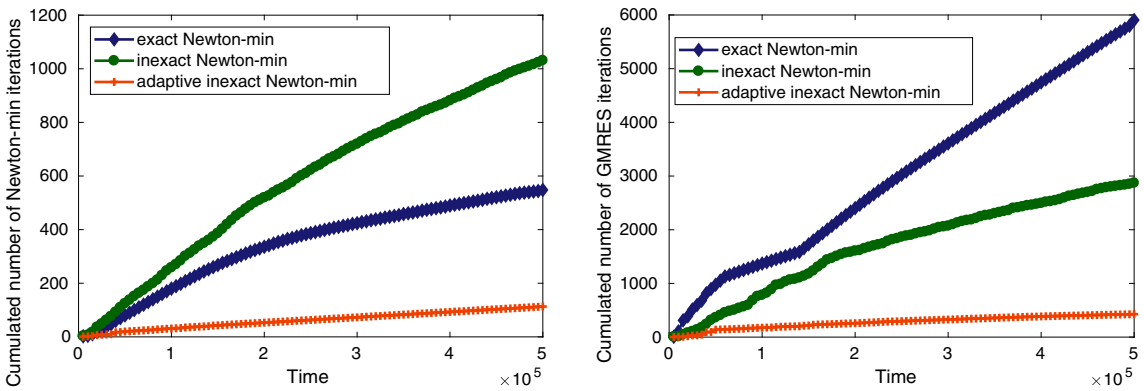

Fig. 7 Cumulated number of Newton-min iterations as a function of time (left), and cumulated number of GMRES iterations as a function of time (right)

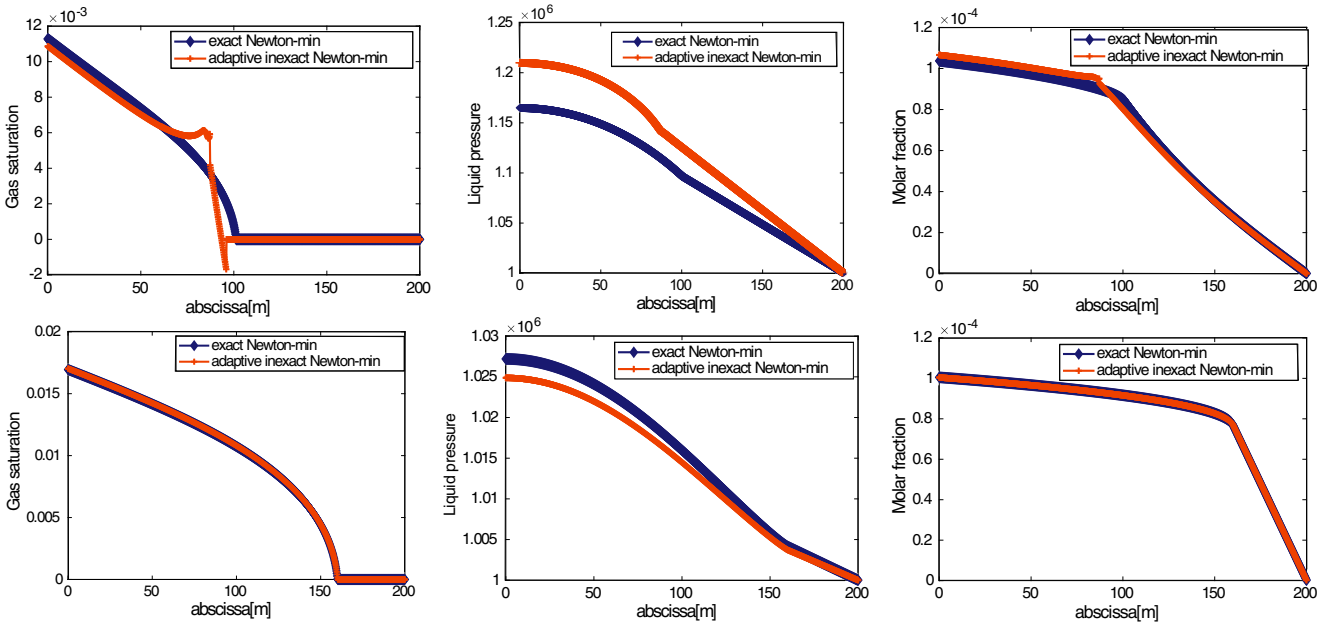

Fig. 8 Gas saturation (top left), liquid pressure (top middle), and molar fraction of liquid hydrogen (top right) for exact Newton-min and adaptive inexact Newton-min at convergence at $t = 1.05 \times 10^5$ years. Gas saturation (bottom left), liquid pressure (bottom middle), and molar fraction of liquid hydrogen (bottom right) for exact Newton-min and adaptive inexact Newton-min at convergence at $t = 3.5 \times 10^5$ years

6.3 Complements

In this section, we carry out numerical simulations supplementing the previous results. We test the influence of the weights γ_{lin} and γ_{alg} on our adaptive inexact semismooth methodology. We also propose a modified version of the inexact Newton-min algorithm where $\Gamma_k = 10^{-4}$ for all Newton-min iterations k (see (97)) and $\varepsilon_{\text{lin}} = 10^{-2}$, and we compare the obtained result with our adaptive inexact Newton-min approach. We also briefly provide results for the adaptive inexact Newton–Fischer–Burmesiter algorithm.

In Table 1, we give the cumulated number of Newton-min iterations and GMRES iterations to reach the end of the simulation for different weights γ_{alg} and γ_{lin}. We observe that decreasing the values of the weights will increase the number of required iterations and increasing the values of the weights, for example $(\gamma_{\text{alg}}, \gamma_{\text{lin}}) = (10^{-1}, 10^{-1})$, will decrease the required number of iterations.

In Fig. 9, we test the influence of the weight γ_{lin} on the behavior of the solution. We take $\gamma_{\text{lin}} = 10^{-6}$, $\gamma_{\text{alg}} = 10^{-3}$, and the time value close to the beginning of the simulation $t = 1.05 \times 10^5$ years when the semismooth Newton solver and the GMRES solver have converged ($k = \bar{k}$, $i = \bar{i}$). Recall that in Fig. 8, we considered the same time instant but with $\gamma_{\text{lin}} = 10^{-3}$. We thus see that the solution given by exact Newton-min and adaptive inexact Newton-min are almost identical with $\gamma_{\text{lin}} = 10^{-6}$. From this example, we deduce that for a time step close to the beginning of the simulation, it is possible to increase the precision in the adaptive inexact resolution by decreasing the value of the weight γ_{lin}. Besides, even taking the smallest values for the weights γ_{lin} and γ_{alg}, $(\gamma_{\text{lin}} = \gamma_{\text{alg}} = 10^{-6})$ will obviously increase the cumulated number of GMRES iterations (2019 iterations see Table 1) and increase the accuracy but, the adaptive strategy is still economic in comparison to exact Newton-min resolution that requires 6000 iterations (see Fig. 7).

Table 1 Total number of linear and nonlinear iterations for adaptive inexact Newton-min method for several parameters γ_{alg} and γ_{lin}

$(\gamma_{\text{alg}}, \gamma_{\text{lin}})$	Cumulated Newton-min iterations	Cumulated GMRES iterations
$(10^{-1}, 10^{-1})$	100	366
$(10^{-3}, 10^{-3})$	113	427
$(10^{-6}, 10^{-3})$	108	967
$(10^{-3}, 10^{-6})$	351	1682
$(10^{-6}, 10^{-6})$	308	2019

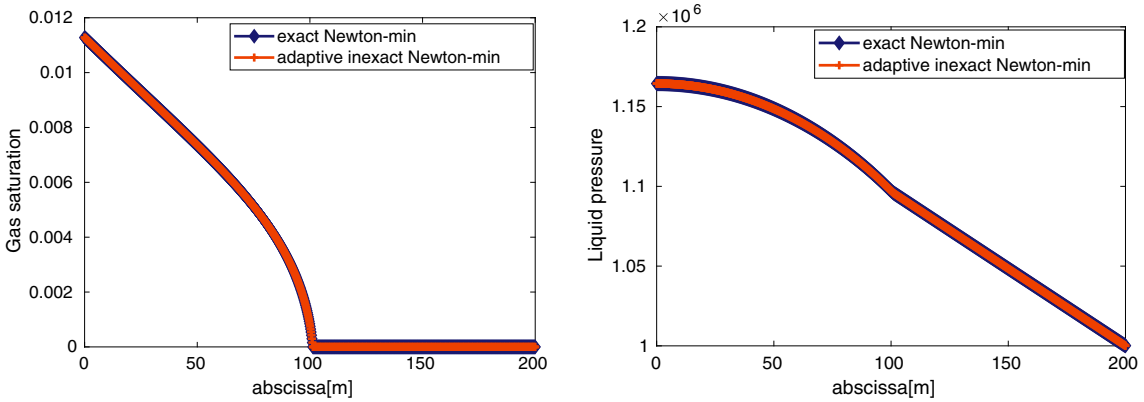

Fig. 9 Gas saturation (left) and liquid pressure (right) for exact Newton-min and adaptive inexact Newton-min at convergence at time $t = 1.05 \times 10^5$ years with $\gamma_{\text{alg}} = 10^{-3}$ and $\gamma_{\text{lin}} = 10^{-6}$. The two curves superimpose

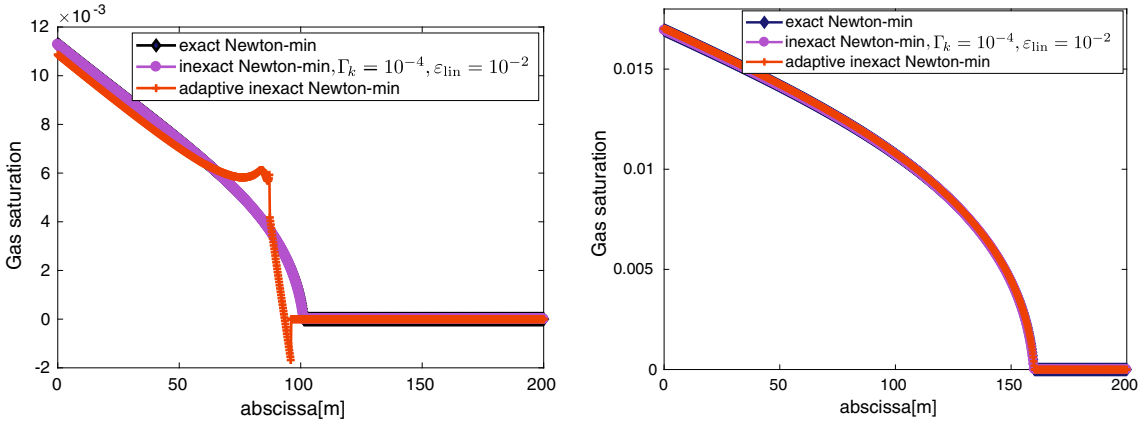

Fig. 10 Gas saturation for exact Newton-min resolution, inexact Newton-min resolution with $\Gamma_k = 10^{-4}$ and $\varepsilon_{\text{lin}} = 10^{-2}$, and adaptive inexact Newton-min resolution at $t = 1.05 \times 10^5$ years (left), and 3.5×10^5 years (right)

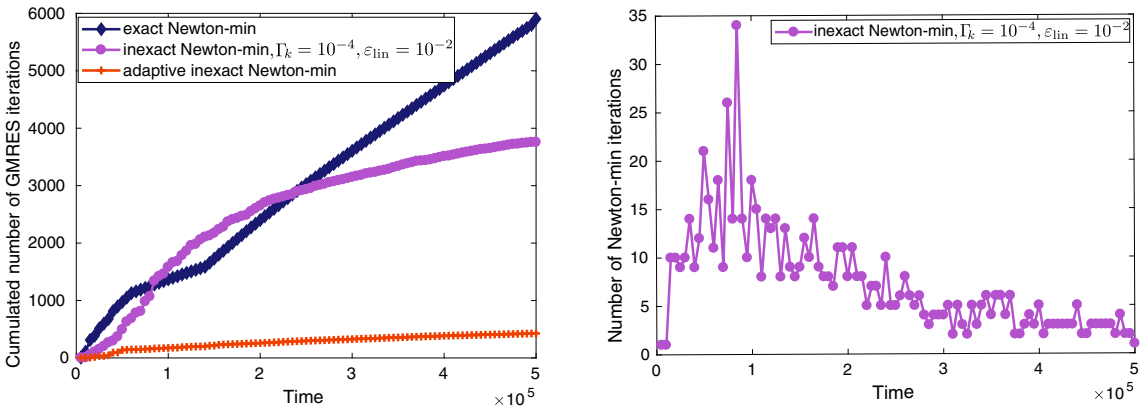

Fig. 11 Cumulated number of Newton-min iterations as a function of time (left) and number of Newton-min iterations at each time step (right)

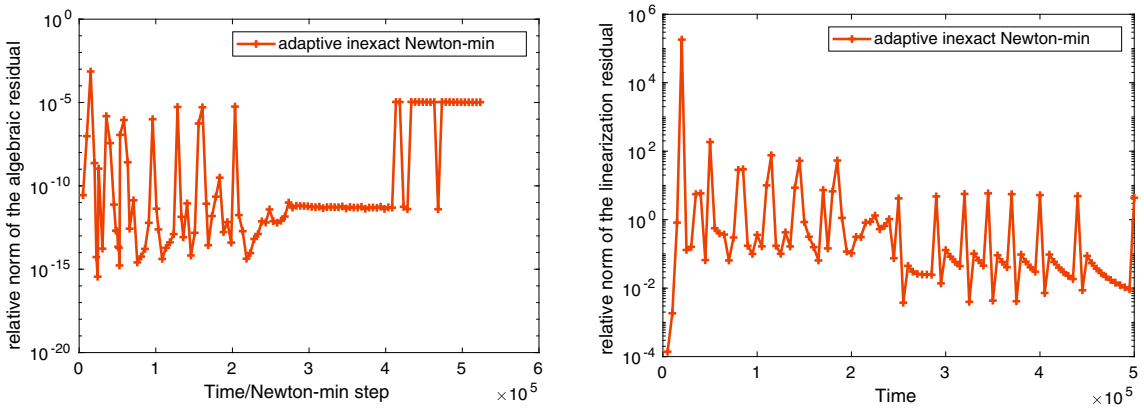

Fig. 12 Relative norm of the algebraic residual when the stopping criterion (91) (a) is satisfied (left) and relative norm of the linearization residual when the stopping criterion (91) (b) is satisfied (right), adaptive inexact Newton-min resolution

In Fig. 10, we illustrate the numerical solution (gas saturation) in the case of the exact Newton-min resolution, the inexact Newton-min resolution with $\Gamma_k = 10^{-4}$ and $\varepsilon_{\text{lin}} = 10^{-2}$, and the adaptive inexact Newton-min resolution of Algorithm 1 with $\gamma_{\text{alg}} = \gamma_{\text{lin}} = 10^{-3}$, for the selected time values $t = 1.05 \times 10^5$ years and 3.5×10^5 years. We observe that the numerical solution given by the inexact resolution is more accurate than the numerical solution given by the adaptive inexact resolution at time $t = 1.05 \times 10^5$ years. However, at the time value $t = 3.5 \times 10^5$ years, the numerical solutions are visually identical.

In Fig. 11, we show the cumulated number of GMRES iterations for three methods as well as the number of required Newton-min iterations at each time step to converge for the inexact Newton-min strategy ($\Gamma_k = 10^{-4}$ and $\varepsilon_{\text{lin}} = 10^{-2}$). We observe an interesting fact: the inexact Newton-min method requires roughly 7 times more cumulated GMRES iterations to converge than the adaptive approach. Note also that at some time instants, the exact Newton-min strategy is cheaper in terms of the cumulated GMRES iterations than the inexact Newton-min approach. This surprising result is explained by the fact that the imposed stopping criterion ($\Gamma_k = 10^{-4}$) is less adequate than the one provided in (97) and thus, the resolution requires more Newton-min iterations at several time step as it is shown in Fig.11 (right). Thus, our adaptive inexact strategy looks as a good compromise as it does not denaturate the numerical solution, preserves the accuracy, and is very economic.

In Fig. 12, we plot the relative norm of the algebraic residual at each Newton-min step within each time step and the relative norm of the linearization residual at each time step for our adaptive inexact Newton-min resolution of Algorithm 1 with $\gamma_{\text{alg}} = \gamma_{\text{lin}} = 10^{-3}$. We see from the right part of Fig.12 that the relative norm of the linearization residual is quite large during the first half of the time iterations. Note that the adaptive criteria based on the estimators are met despite these large residuals (we recall there can be a large shift between linearization residual and linearization estimators curves, see Fig. 4). This explains why the solution given by this inexact Newton-min resolution with the criteria $\Gamma_k = 10^{-4}$ and $\varepsilon_{\text{lin}} = 10^{-2}$ is more accurate than the solution given by our adaptive approach at $t = 1.05 \times 10^5$ years.

Overall, however, the adaptive inexact Algorithm 1 allows to find automatically the suitable (relative) balance between the error components, which results into variable absolute values of the relative linearization and relative algebraic residuals observed in Fig. 12, and leads to a good compromise between the accuracy and the computational cost.

To conclude this section, we present some results obtained by the Newton–Fischer–Burmeister algorithm. In this case, the nonlinear complementarity constraints can be

Table 2 Total number of nonlinear and linear iterations for the adaptive inexact Newton–Fischer–Burmeister method for several parameters γ_{alg} and γ_{lin} and for the exact Newton–Fischer–Burmeister method

$(\gamma_{\text{alg}}, \gamma_{\text{lin}})$	Cumulated number of Newton–Fischer–Burmeister iterations	Cumulated number of GMRES iterations
$(10^{-1}, 10^{-1})$	100	428
$(10^{-3}, 10^{-3})$	119	751
$(10^{-3}, 10^{-6})$	482	2074
$(10^{-6}, 10^{-3})$	117	1694
Exact resolution	757	10089

reformulated thanks to the semismooth Fischer–Burmeister function (see 32) as follows: $\forall K \in \mathcal{T}_h$, $\forall 1 \leq n \leq N_t$,

$$\begin{aligned} &1 - S_K^n \geq 0, \quad H\left[P_K^n + P_{\mathrm{cp}}(S_K^n)\right] - \beta^1 \chi_K^n \geq 0, \\ &\left[1 - S_K^n\right]\left[H\left[P_K^n + P_{\mathrm{cp}}(S_K^n)\right] - \beta^1 \chi_K^n\right] = 0, \\ &\Longleftrightarrow \; f_{\mathrm{FB}}(1 - S_K^n, H\left[P_K^n + P_{\mathrm{cp}}(S_K^n)\right] - \beta^1 \chi_K^n) = 0. \end{aligned}$$

Table 2 provides the behavior of the exact Newton–Fischer–Burmeister algorithm and of the adaptive inexact Newton–Fischer–Burmeister algorithm for several weights γ_{alg} and γ_{lin}. The adaptive strategy gives suitable results as it roughly saves 90% of the iterations in comparison with the exact resolution. Furthermore, we can observe that exact and adaptive inexact Newton-min provides better results in terms of computational cost than exact and adaptive inexact Newton–Fischer–Burmeister. This observation is in agreement with the fast convergence rate of the Newton-min algorithm [12, 37, 38].

7 Conclusion

We have studied a compositional two-phase liquid–gas flow with appearance/disappearance of the gas phase. We have employed the semismooth theory to treat the nonlinearities in the complementarity constraints. We have devised a posteriori error estimates between the exact and approximate solution, in particular when the phase transition occurs and we have distinguished the different error components. In the numerical experiments, we have tested the quality of our adaptive strategy. In particular, the results confirmed the strength of this approach.

Acknowledgments We thank S. Yousef (IFPEN) for discussions on a posteriori error estimates and implementation.

Funding information This project has received funding from the European Research Council (ERC) under the European Union's Horizon 2020 research and innovation program (grant agreement no. 647134 GATIPOR).

References

1. Ainsworth, M., Oden, J.T.: A Posteriori Error Estimation in Finite Element Analysis. Pure and Applied Mathematics. Wiley-Interscience [John Wiley & Sons], New York (2000)
2. Amaziane, B., Jurak, M., Žgaljić Keko, A.: Modeling compositional compressible two-phase flow in porous media by the concept of the global pressure. Comput. Geosci. **18**(3-4), 297–309 (2014). https://doi.org/10.1007/s10596-013-9362-2
3. Antontsev, S.N., Kazhikhov, A.V., Monakhov, V.N.: Boundary Value Problems in Mechanics of Nonhomogeneous Fluids, Studies in Mathematics and its Applications, vol. 22. North-Holland Publishing Co., Amsterdam (1990). Translated from the Russian
4. Arbogast, T.: The existence of weak solutions to single porosity and simple dual-porosity models of two-phase incompressible flow. Nonlinear Anal. **19**(11), 1009–1031 (1992). https://doi.org/10.1016/0362-546X(92)90121-T
5. Arioli, M., Georgoulis, E.H., Loghin, D.: Stopping criteria for adaptive finite element solvers. SIAM J. Sci. Comput. **35**(3), A1537–A1559 (2013). https://doi.org/10.1137/120867421
6. Bastian, P.: Numerical computation of multiphase flow in porous media. Habilitationsschrift (1999)
7. Bebendorf, M.: A note on the Poincaré inequality for convex domains. Z. Anal. Anwendungen **22**(4), 751–756 (2003). https://doi.org/10.4171/ZAA/1170
8. Ben Belgacem, F., Bernardi, C., Blouza, A., Vohralík, M.: On the unilateral contact between membranes. Part 2: A posteriori analysis and numerical experiments. IMA J. Numer. Anal. **32**(3), 1147–1172 (2012). https://doi.org/10.1093/imanum/drr003
9. Ben Gharbia, I., Gilbert, J.: Nonconvergence of the plain Newton-min algorithm for linear complementarity problems with a P-matrix. Math. Program. **134**, 349–364 (2012). https://doi.org/10.1007/s10107-010-0439-6
10. Ben Gharbia, I., Gilbert, J.: An algorithmic characterization of P-matricity. SIAM J. Matrix Anal. Appl. **34**(3), 904–916 (2013). https://doi.org/10.1137/120883025
11. Ben Gharbia, I., Gilbert, J.: An algorithmic characterization of P-matricity II: Adjustments, refinements, and validation. SIAM J. Matrix Anal. Appl. **40**(2), 800–813 (2019). https://doi.org/10.1137/18M1168522
12. Ben Gharbia, I., Jaffré, J.: Gas phase appearance and disappearance as a problem with complementarity constraints. Math. Comput. Simul. **99**, 28–36 (2014). https://doi.org/10.1016/j.matcom.2013.04.021
13. Bonnans, J.F., Gilbert, J.C., Lemaréchal, C., Sagastizábal, C.A. Numerical Optimization, Universitext, 2nd edn. Springer, Berlin (2006). Theoretical and practical aspects
14. Bourgeat, A., Mladen, J., Smaï, F.: Two-phase, partially miscible flow and transport modeling in porous media; Application to gas migration in a nuclear waste repository. Comput. Geosci. **13**(5), 29–42 (2009)
15. Braess, D., Schöberl, J.: Equilibrated residual error estimator for edge elements. Math. Comp. **77**(262), 651–672 (2008). https://doi.org/10.1090/S0025-5718-07-02080-7
16. Brezzi, F., Fortin, M.: Mixed and Hybrid Finite Element Methods. Springer Series in Computational Mathematics, vol. 15. Springer, New York (1991)
17. Cancès, C., Pop, I.S., Vohralík, M.: An a posteriori error estimate for vertex-centered finite volume discretizations of immiscible incompressible two-phase flow. Math. Comp. **83**(285), 153–188 (2014). https://doi.org/10.1090/S0025-5718-2013-02723-8
18. Chavent, G., Jaffré, J.: Mathematical models and finite elements for reservoir simulation. North Holland. https://doi.org/10.1016/j.matcom.2013.04.021 (1986)
19. Chen, Z.: Degenerate two-phase incompressible flow. I. Existence, uniqueness and regularity of a weak solution. J. Diff. Equ. **171**(2), 203–232 (2001). https://doi.org/10.1006/jdeq.2000.3848
20. Chen, Z.: Reservoir Simulation, CBMS-NSF Regional Conference Series in Applied Mathematics, vol. 77. Society for Industrial and Applied Mathematics (SIAM), Philadelphia (2007). Mathematical techniques in oil recovery
21. Chen, Z., Huan, G., Ma, Y.: Computational Methods for Multiphase Flows in Porous Media. Computational Science & Engineering, vol. 2. Society for Industrial and Applied Mathematics (SIAM), Philadelphia (2006)
22. Chen, Z., Nochetto, R.H.: Residual type a posteriori error estimates for elliptic obstacle problems. Numer. Math. **84**(4), 527–548 (2000). https://doi.org/10.1007/s002110050009

23. Chippada, S., Dawson, C.N., Martinez, M.L., Wheeler, M.F.: A Godunov-type finite volume method for the system of shallow water equations. Comput. Methods Appl. Mech. Engrg. **151**(1–2), 105–129 (1998). https://doi.org/10.1016/S0045-7825(97)00108-4. Symposium on Advances in Computational Mechanics, Vol. 3 (Austin, TX, 1997)
24. Clarke, F.H. Optimization and Nonsmooth Analysis. Classics in Applied Mathematics, 2nd edn., vol. 5. Society for Industrial and Applied Mathematics (SIAM), Philadelphia (1990)
25. Class, H., Helmig, R., Bastian, P.: Numerical simulation of non-isothermal multiphase multi-component processes in porous media. 1. An efficient solution technique. Adv. Water. Resour. **25**, 533–550 (2002)
26. Dabaghi, J., Martin, V., Vohralík, M.: Adaptive inexact semismooth Newton methods for the contact problem between two membranes. https://hal-enpc.archives-ouvertes.fr/hal-01666845/document. HAL Preprint 01666845, submitted for publication (2018)
27. Dembo, R.S., Eisenstat, S.C., Steihaug, T.: Inexact Newton methods. SIAM J. Numer. Anal. **19**(2), 400–408 (1982). https://doi.org/10.1137/0719025
28. Destuynder, P., Métivet, B.: Explicit error bounds in a conforming finite element method. Math. Comp. **68**(228), 1379–1396 (1999). https://doi.org/10.1090/S0025-5718-99-01093-5
29. Di Pietro, D.A., Flauraud, E., Vohralík, M., Yousef, S.: A posteriori error estimates, stopping criteria, and adaptivity for multiphase compositional Darcy flows in porous media. J. Comput. Phys. **276**, 163–187 (2014). https://doi.org/10.1016/j.jcp.2014.06.061
30. Di Pietro, D.A., Vohralík, M., Yousef, S.: An a posteriori-based, fully adaptive algorithm with adaptive stopping criteria and mesh refinement for thermal multiphase compositional flows in porous media. Comput. Math. Appl. **68**(12, part B), 2331–2347 (2014). https://doi.org/10.1016/j.camwa.2014.08.008
31. Eisenstat, S.C., Walker, H.F.: Globally convergent inexact Newton methods. SIAM J. Optim. **4**(2), 393–422 (1994). https://doi.org/10.1137/0804022
32. Ern, A., Vohralík, M.: Adaptive inexact Newton methods with a posteriori stopping criteria for nonlinear diffusion PDEs. SIAM J. Sci. Comput. **35**(4), A1761–A1791 (2013). https://doi.org/10.1137/120896918
33. Ern, A., Vohralík, M.: Polynomial-degree-robust a posteriori estimates in a unified setting for conforming, nonconforming, discontinuous Galerkin, and mixed discretizations. SIAM J. Numer. Anal. **53**(2), 1058–1081 (2015). https://doi.org/10.1137/130950100
34. Eymard, R., Gallouët, T., Herbin, R.: Finite Volume Methods. Handb. Numer. Anal., VII. North-Holland (2000)
35. Eymard, R., Herbin, R., Michel, A.: Mathematical study of a petroleum-engineering scheme. M2AN Math. Model. Numer. Anal. **37**(6), 937–972 (2003). https://doi.org/10.1051/m2an:2003062
36. Facchinei, F., Kanzow, C.: A nonsmooth inexact Newton method for the solution of large-scale nonlinear complementarity problems. Math. Programming **76**(3, Ser. B), 493–512 (1997). https://doi.org/10.1016/S0025-5610(96)00058-5
37. Facchinei, F., Pang, J.S.: Finite-Dimensional Variational Inequalities and Complementarity Problems. Springer Series in Operations Research, vol. I. Springer, New York (2003)
38. Facchinei, F., Pang, J.S.: Finite-Dimensional Variational Inequalities and Complementarity Problems. Springer Series in Operations Research, vol. II. Springer, New York (2003)
39. Falta, R.W., Pruess, K., Javandel, I., Witherspoon, P.: Numerical modeling of steam injection for the removal of nonaqeous phase liquids from the subsurface. Water. Resour. Res **28**(1. Numerical formulation), 433–449 (1992)
40. Ge, Z., Ni, Q., Zhang, X.: A smoothing inexact Newton method for variational inequalities with nonlinear constraints. J. Inequal. Appl. pp. Paper **160**, 12 (2017). https://doi.org/10.1186/s13660-017-1433-9
41. Gross, S., Reusken, A.: Numerical Methods for Two-Phase Incompressible Flows. Springer Series in Computational Mathematics, vol. 40. Springer, Berlin (2011)
42. Helmig, R.: Multiphase flow and transport processes in the subsurface–A contribution to the modeling of hydrosystems (1997)
43. Huber, R., Helmig, R.: Node-centered finite volume discretizations for the numerical simulation of multiphase flow in heterogeneous porous media. Comput. Geosci. **4**(2), 141–164 (2000). https://doi.org/10.1023/A:1011559916309
44. Jiránek, P., Strakoš, Z., Vohralík, M.: A posteriori error estimates including algebraic error and stopping criteria for iterative solvers. SIAM J. Sci. Comput. **32**(3), 1567–1590 (2010). https://doi.org/10.1137/08073706X
45. Kanzow, C.: Inexact semismooth Newton methods for large-scale complementarity problems. Optim. Methods Softw. **19**(3–4), 309–325 (2004). https://doi.org/10.1080/10556780310001636369. The First International Conference on Optimization Methods and Software. Part II
46. Karakashian, O.A., Pascal, F.: A posteriori error estimates for a discontinuous Galerkin approximation of second-order elliptic problems. SIAM J. Numer. Anal. **41**(6), 2374–2399 (2003). https://doi.org/10.1137/S0036142902405217
47. Kelley, C.T.: Iterative Methods for Linear and Nonlinear Equations. Frontiers in Applied Mathematics, vol. 16. Society for Industrial and Applied Mathematics (SIAM), Philadelphia (1995)
48. Kornhuber, R.: A posteriori error estimates for elliptic variational inequalities. Comput. Math. Appl. **31**(8), 49–60 (1996). https://doi.org/10.1016/0898-1221(96)00030-2
49. Kroener, D., Luckhaus, S.: Flow of oil and water in a porous medium. J. Diff. Equ. **55**(2), 276–288 (1984). https://doi.org/10.1016/0022-0396(84)90084-6
50. Lacroix, S., Vassilevski, Y., Wheeler, J., Wheeler, M.: Iterative solution methods for modeling multiphase flow in porous media fully implicitly. SIAM J. Sci. Comput. **25**(3), 905–926 (2003). https://doi.org/10.1137/S106482750240443X
51. Ladevèze, P.: Comparaison de modèles de mécanique des milieux continus. Thèse d'état, Université Paris VI Paris (1975)
52. Lauser, A., Hager, C., Helmig, R., Wohlmuth, B.: A new approach for phase transitions in miscible multi-phase flow in porous media. Adv. Water Resour. **68**, 957–966 (2011)
53. Martínez, J.M., Qi, L.Q.: Inexact Newton methods for solving nonsmooth equations. J. Comput. Appl. Math. **60**(1–2), 127–145 (1995). https://doi.org/10.1016/0377-0427(94)00088-I. Linear/nonlinear iterative methods and verification of solution (Matsuyama, 1993)
54. Meidner, D., Rannacher, R., Vihharev, J.: Goal-oriented error control of the iterative solution of finite element equations. J. Numer. Math. **17**(2), 143–172 (2009). https://doi.org/10.1515/JNUM.2009.009
55. Niessner, J., Helmig, R.: Multi-scale modeling of three-phase-three-component processes in heterogeneous porous media. Adv. Water Resour. **30**, 2309–2325 (2007)
56. Panfilov, M., Panfilova, I.: Method of negative saturations for flow with variable number of phases in porous media: Extension to three-phase multi-component case. Comput. Geosci. **18**(5), 385–399 (2014)
57. Panfilov, M., Rasoulzadeh, M.: Interfaces of phase transition and disappearance and method of negative saturation for compositional flow with diffusion and capillarity in porous media. Transp. Porous. Med **83**(5), 73–98 (2010)
58. Papež, J., Rüde, U., Vohralík, M., Wohlmuth, B.: Sharp algebraic and total a posteriori error bounds for h and p finite elements via

a multilevel approach. https://hal.inria.fr/hal-01662944/en. HAL Preprint 01662944, submitted for publication (2017)
59. Payne, L.E., Weinberger, H.F.: An optimal Poincaré inequality for convex domains. Arch. Rational Mech. Anal. **5**, 286–292 (1960). https://doi.org/10.1007/BF00252910
60. Pop, I.S., Radu, F., Knabner, P.: Mixed finite elements for the Richards' equation: Linearization procedure. J. Comput. Appl. Math. **168**(1-2), 365–373 (2004). https://doi.org/10.1016/j.cam.2003.04.008
61. Prager, W., Synge, J.L.: Approximations in elasticity based on the concept of function space. Quart. Appl. Math. **5**, 241–269 (1947). https://doi.org/10.1090/qam/25902
62. Radu, F.A., Kumar, K., Nordbotten, J.M., Pop, I.S.: A robust, mass conservative scheme for two-phase flow in porous media including Hölder continuous nonlinearities. IMA J. Numer. Anal. **38**(2), 884–920 (2018). https://doi.org/10.1093/imanum/drx032
63. Raviart, P.A., Thomas, J.M.: A Mixed Finite Element Method for 2nd Order Elliptic Problems, vol. 606, pp. 292–315. Lecture Notes in Math. (1977)
64. Repin, S.: A Posteriori Estimates for Partial Differential Equations. Radon Series on Computational and Applied Mathematics, vol. 4. Walter de Gruyter GmbH & Co. KG, Berlin (2008)
65. Repin, S.I.: Functional a posteriori estimates for elliptic variational inequalities. Zap. Nauchn. Sem. S.-Peterburg. Otdel. Mat. Inst. Steklov. (POMI) **348**((Kraevye Zadachi Matematicheskoĭ Fiziki i Smezhnye Voprosy Teorii Funktsiĭ. 38)), 147–164, 305 (2007). https://doi.org/10.1007/s10958-008-9093-4
66. Roberts, J.E., Thomas, J.M.: Mixed and hybrid methods. In: Handbook of Numerical Analysis, vol. II, pp. 523–639. North-Holland (1991)
67. Sboui, A., Jaffré, J.: Henry' law and gas phase disappearance. Transp. Porous Media **82**, 521–526 (2010)
68. Sha, W.T.: Novel Porous Media Formulation for Multiphase Flow Conservation Equations. Cambridge University Press, Cambridge (2011). With forewords by Alan Schriesheim, Wm. Howard Arnold and Charles Kelber
69. Slodička, M.: A robust and efficient linearization scheme for doubly nonlinear and degenerate parabolic problems arising in flow in porous media. SIAM J. Sci. Comput. **23**(5), 1593–1614 (2002). https://doi.org/10.1137/S1064827500381860
70. Veeser, A.: Efficient and reliable a posteriori error estimators for elliptic obstacle problems. SIAM J. Numer. Anal. **39**(1), 146–167 (2001). https://doi.org/10.1137/S0036142900370812
71. Vohralík, M.: Residual flux-based a posteriori error estimates for finite volume and related locally conservative methods. Numer. Math. **111**(1), 121–158 (2008). https://doi.org/10.1007/s00211-008-0168-4
72. Vohralík, M., Wheeler, M.F.: A posteriori error estimates, stopping criteria, and adaptivity for two-phase flows. Comput. Geosci. **17**(5), 789–812 (2013). https://doi.org/10.1007/s10596-013-9356-0